UNIVERSITY OF CALIFORNIA SAN DIEGO

Utilization of forward and reverse genetics to identify genes involved in stress responses in the model organisms *Brachypodium distachyon* and *Arabidopsis thaliana*

A thesis submitted in partial satisfaction of the requirements of the degree Master of Science

in

Biology

by

Bryn Nicole Kuluehu Lopez

Committee in charge:

Professor Julian I Schroeder, Chair
Professor Alisa Huffaker
Professor Yunde Zhao

2020

The Thesis of Bryn Nicole Kuluehu Lopez is approved, and it is acceptable in quality and form for publication on microfilm and electronically.

Chair

University of California San Diego

2020

DEDICATION

I grew up hearing “It takes a village to raise a child”, and I could not agree more. I would like to dedicate this thesis to my village; all the friends and family that have supported me now and throughout my life, especially my parents. I could not have gotten this far without your continued love and support, you all inspire me to continue trying my best even when I doubt myself.

TABLE OF CONTENTS

LIST OF FIGURES

LIST OF TABLES

ACKNOWLEDGEMENTS

I would like to acknowledge Professor Julian Schroder for his support as the chair of my committee. He welcomed me into the lab as a senior during my undergraduate studies, and has facilitated my learning of so many different techniques by allowing me to join such a prestigious and highly productive lab.

I am also endlessly thankful for the entire "Brachy Team" and all of the members. Morgana Sidhom for her help on both projects in Chapter 1 and 2. Along with Felipe Rangel, my friend and teammate while working on the forward genetic screen. And especially, Dr. Paulo H. O. Ceciliato, my mentor, whose guidance has been immeasurably helpful in my development as a scientist. Paulo, thank you for always encouraging me to do the best work I could, being endlessly patient, and teaching me not just how to do experiments; but how to be a scientist. I will always be grateful for your guidance, dedication, and encouragement. Obrigada Paulo!

Chapter 1 is co-authored with Dr. Paulo Ceciliato, Felipe Rangel, Morgana Sidhom, and Li Zhang. Chapter 2 is co-authored with Morgana Sidhom. Chapter 3 is co-authored with Dr. Paulo Ceciliato. The thesis author was the primary author of these chapters.

ABSTRACT OF THE THESIS

Utilization of forward and reverse genetics to identify genes involved in stress responses in the model organisms *Brachypodium distachyon* and *Arabidopsis thaliana*

by

Bryn Nicole Kuluehu Lopez

Master of Science in Biology

University of California San Diego, 2020

Professor Julian Schroeder, Chair

Plants face various biotic and abiotic stresses in their environment and must be able to rapidly respond to such stresses. Some of the major abiotic stresses affecting plants include drought, salinity, heavy metals, and increasing atmospheric CO_2 concentrations. These stresses contribute to worldwide food shortages caused by yield penalties and loss of crop plants. The rapidly rising atmospheric CO_2 concentrations, which have reached the highest level observed in human history, have already begun affecting all life on earth, including plants. Increased CO_2

affects plants directly by triggering stomatal closure, and indirectly by influencing continually more extreme weather patterning. More than 80% of the worlds consumed calories are from crop plants, which are already experiencing almost 1% in yield penalties. Food insecure and developing countries have already been disproportionately affected by the decline in available food supply, which is predicted to worsen. Yield and grain filling penalties are observed due to the stress response of plants beginning with the most common and rapid response being closure of stomata. Stomata are pores present on the surface of leaves allowing for gas exchange with the surrounding environment. Stomata will close to a multitude of stimuli, but two that have been especially prevalent in the face of climate change include closure as a response to CO_2, and ABA, a phytohormone produced in the presence of drought. In order to feed an ever-growing global population, mutants displaying reduced sensitivities to stresses must be identified. In an effort to identify mutant lines that may be resistant to stressors, both forward and reverse genetics screens were utilized in two different model organisms. To this end, work in new model organism *Brachypodium distachyon* has been done in an effort to identify novel genes involved in CO_2 signaling. *Brachypodium distachyon* was also utilized in a reverse genetic screen to determine if the same components involved in stomatal development in *Arabidopsis thaliana* contributed in the same manner in grasses. Characterization of a mutant identified in a screen of ABA insensitive *Arabidopsis thaliana* has also been pursued and may lead to identification of important signaling components involved in drought responses. Identification of causative mutations conferring reduced sensitivity to ABA or increased CO_2 concentration may be crucial in generating crop plants with lessened yield penalties in the face of the changing global climate to continue feeding the growing human population.

Chapter 1 Characterization of *chill* mutant lines identified in *Brachypodium distachyon* forward genetic screen

Plants have evolved mechanisms to rapidly respond to their ever-changing environment, one of which being the ability to open and close pores on the leaf surfaces called stomata. Through these pores they are able to conduct gas exchange with their environment, allowing them to take up CO_2 and release O_2 and water vapor into the atmosphere. Stomata close under

stressful conditions, and the loss of the ability to release water vapor leads to warmer leaf temperatures, which can be measured through thermal imaging. Stomata in grasses are made up of two dumbbell-shaped guard cells that work counteractively with the surrounding subsidiary cells, and together they regulate stomatal movement. While the CO_2 signaling pathway has been extensively studied in current model organism *Arabidopsis thaliana*, it is not as well known in grasses, which include some of the major cereal crops such as wheat and rye. In an effort to identify more key components involved in the regulation of this pathway, a forward genetic screen was initiated, looking for mutants with disrupted responses to high-CO_2 induced stomatal closure. Several promising lines have been identified in this screen, and characterization is well underway for those shown to be most robust based on initial results. Lines identified in the screen include 3 independent mutant lines which have been shown to be heavily impaired in stomatal closure induced by high CO_2, yet still respond to ABA, as shown through intact leaf gas exchange analyses. Characterization of the most promising line has been pursued including backcrossing to the wildtype and generation of the F2 mapping population, which will be used to identify the causative mutation utilizing both WGS and BSA. Identification of the causative mutation may allow for generation of cereal crop plants displaying higher photosynthetic and carbon fixation rates even in the presence of increased CO_2. Plants that do not close stomata under high CO_2 conditions may be less at risk of suffering heat stress and reduced yield and grain filling due to reduced photosynthesis. Implementation of identified genes in cereal crops may potentially prevent additional stress on plants created by increased atmospheric CO_2, prevention of which will be necessary to sustainably generate enough food for a continuously growing human population.

1.1 Introduction:

Atmospheric CO_2 concentrations have surpassed the highest recorded concentration seen in human history. Through approximately the last 800,000 years, atmospheric CO_2 concentrations have remained at about 300 ppm; however, concentrations have spiked beginning in the industrial revolution and are currently near 410 ppm (https://scripps.ucsd.edu/programs/keelingcurve/). Elevated CO_2 conditions is one of the major contributors of climate change observed around the world and concentrations continue to elevate at an unprecedented speed of approximately 1.0 mmol mol^{-1} annually as carbon emissions continue to rise (Headquarters, 2014; Stocker et al., 2013)

This increased atmospheric CO_2 concentration may also be contributing to global food insecurity as it reduces both crop growth and yield, negatively impacting agriculture (Zheng et al., 2019). Crop productivity is also indirectly affected by rising CO_2 concentrations as this also increases frequency, duration, and intensity of heat waves putting crops at risk of heat stress, including major cereal crop wheat (Asseng et al., 2015; Wahid et al., 2007). This increase in global temperature has often been attributed to the heat trapping nature of CO_2, which is becoming particularly detrimental as atmospheric concentration continues to increase. In the presence of climate change, occurrence and severity of drought stress is expected to increase which can negatively impact plant development and reproduction, especially in cool-season plants (Sherrard & Maherali, 2006).

Plants can perceive these changes in the environment and adapt their physiology in order to maximize growth and reproduction. Stomata are pores on the surface of leaves which facilitate gas exchange between the plant and surrounding environment. Stomata are surrounded by guard cells which control opening and closing by increasing or decreasing relative turgor pressure

(Willmer et al., 1996). Turgor pressure is mediated by ion and water movement across guard cell membranes, where increasing pressure leads to stomatal opening (Kollist et al., 2014). Under high CO_2 conditions plants generally show lessened stomatal conductance, which also leads to lessened photosynthetic rates over time when grown under increased CO_2 (Kanemoto et al. 2009; Xu et al. 2016).

Stomatal closure induced by high CO_2 is observed due to a signal cascade initiated as CO_2 enters the guard cells, ultimately leading to decreased turgor pressure. *PIP2* is an aquaporin through which CO_2 can enter the cell. PIP also interacts with *βCA4* (Beta Carbonic Anhydrase 4), leading to accelerated HCO_3- (bicarbonate) formation (C. Wang et al., 2015). CO_2 and HCO_3- upregulate *MPK4/12* (Mitogen Activated Protein Kinase 4/12), inhibiting downstream *HT1* (High Leaf Temperature 1). *MAP4* and *MAP12* have both been established as essential regulators in triggering downstream stomatal closure in response to high CO_2 and contribute to closure even in the absence of *RHC1* (Resistant to High CO_2) (Tõldsepp et al., 2018). When active, *HT1* leads to downstream activation of *CBC1/2* (Convergence of blue light and CO_2), both of which work together to trigger stomatal opening by inhibiting *SLAC1* (Slow Anion Channel Associated 1). *SLAC1* is upregulated by *GHR1* (Guard Cell Hydrogen Peroxide-Resistant 1), and when *SLAC1* is active, it promotes stomatal closure. *SLAC1* is required for CO_2 regulated stomatal closure and has been proposed to function as a bicarbonate sensor, responding to increased intracellular CO_2/bicarbonate concentrations. Closure is promoted by opening of *SLAC1* allowing anions to flow out of the cell depolarizing the membrane, triggering opening of K+ channels causing an efflux of K+ ions and water, leading to decreased turgor pressure inside the cell leading to stomatal closure (Zhang et al., 2018).

When plants perceive stress triggering stomatal closure, reduced evapotranspiration can be observed (Zhang et al., 2018). Evapotranspiration is mediated by stomata, allowing the release of water vapor and oxygen into the atmosphere while taking up CO_2, which allows the plant to cool canopy temperature to combat heat stress (Hetherington and Woodward 2003; Harrison et al. 2020). Yield penalties are observed due to stomatal closure, or narrowing of stomata observed under stress conditions, such as increased CO_2 or the presence of phytohormones such as ABA (abscisic acid) (Ainsworth & Rogers, 2007; Engineer et al., 2016).

Currently, the most common model organism used in plant biology is *Arabidopsis thaliana.* It has become well established as such due to its small size, short lifespan, and it has already been extensively characterized, including genome mapping(Kaul et al. 2000; A. W. Woodward and Bartel 2018). While *Arabidopsis thaliana* is frequently used as the model organism for dicots, it is known to be fundamentally different from important cereal crops such as wheat. In this regard, *Brachypodium distachyon*, a grass, has been proposed as a new model for monocots (Scholthof et al., 2018). Brachypodium has been proposed as a better reference model organism for its evolutionary similarity to major cereal crops such as wheat and rye, even more so than previous model organism, rice (Brkljacic et al., 2011). Not only is Brachypodium more evolutionarily similar to cereal crops than rice, it is also much smaller and has a shorter life span making it much more favorable (Brkljacic et al. 2011; Scholthof et al. 2018). Brachypodium has a very small genome of only about 300Mb, making it suitable for high-throughput screening (Huo et al., 2009). Further work with Brachypodium may lead to important advancements in counteracting food insecurity and maintaining sustainable food supply (Vogel et al., 2010).

Grasses are different from dicots for a multitude of reasons, but an important distinction is that grasses contain dumbbell shaped guard cells unlike the kidney shaped cells surrounding the

stomata of dicots. It has been suggested that this shape may make them more efficient at responding to changes in the environment due to their distinctive shape; requiring less movement of ions across membranes to adjust turgor pressure (Raschke and Fellows 1971; Hetherington and Woodward 2003). Similarly to dicots, stomata will close under stress such as high CO_2 or drought conditions leading to less evapotranspiration and increasing risk of heat stress (Hetherington and Woodward 2003; Fahad et al. 2017). Heat stress can lead to yield penalties and lower biomass of mature plants (Fahad et al., 2017).

Thermal imaging can be used to measure the differences between canopy leaf temperature between mutants containing stomata impaired in closure under high CO_2 conditions when compared to wildtype lines. Thermal imaging is a useful method of high throughput screening of large mutant populations in a non-invasive manner by exploiting the differences in canopy leaf temperature (Yibing Wang et al., 2004). The differences in leaf temperature are assumed to be due to stomatal impairments, if colder mutants are identified under stressful conditions that are known to cause to stomatal closure, it may be indicative of novel genes implicated in CO_2 or ABA responses (Yibing Wang et al., 2004). In order to find new genes/proteins involved in stomatal responses to high CO_2 in grasses, a forward genetic screen was pursued using a population of plants mutagenized by EMS (ethyl-methyl sulfonate). This was done through thermal imaging of mutagenized plants under both ambient (400 ppm) and high CO_2 conditions (900 ppm) alongside wildtype controls in the same background (Bd 21-3). 50 lines were selected through this method in the M5 generation; however, only 28 lines could be reconfirmed in the same generation. Initiation of a tertiary screen lead to exclusion of the 7 that were screened as they appeared wildtype. The remaining 21 henceforth will be referred to as *chill1-21*. Additional characterization of mutant phenotypes included gas exchange analyses for comparative analysis of stomatal

conductance capabilities. Back crossing to the wildtype control (Bd 21-3), or to other mutants to determine allelism has also been initiated but has not yet been completed for all lines of interest.

1.2 Results:

1.2.1 Characterization of the most promising chill mutant lines

Due to rising atmospheric CO_2 concentrations, there is a need for plants that do not suffer yield consequences or overheat due to excessive stomatal closure. Exposure to high concentrations of CO_2 leads to closure of stomatal pores on the surface of leaves. Stomatal pores facilitate gas exchange for photosynthesis and allow plants to go through evapotranspiration. Evapotranspiration, in turn, allows for the plant to reduce the canopy leaf temperature through water loss. Water is released as vapor through the stomatal pores, and as the water evaporates it causes the leaf to cool, preventing heat stress. Therefore, plants that have more closed stomata resulting from exposure to high CO_2 concentrations lose less water through evapotranspiration; and will have higher canopy leaf temperatures (Engineer et al., 2014). This increased leaf temperature can be measured using an infra-red thermal camera. Thermal imaging analysis allows for identification of colder mutants and visualization of temperature differences between lines. Those that appear cooler in thermal images may have impairments in stomatal closing, causing stomatal pores to remain more open, close slower, or both. Impairments in stomatal closing may be beneficial as atmospheric concentrations rise, as those mutants may be less likely to suffer from heat stress caused by lessened evapotranspiration.

In an effort to identify mutants that may be impaired in stomatal movement, a forward genetic screen of a library of EMS (ethyl-methyl sulfonate) mutagenized lines was completed by previous team members. Approximately 1305 mutant lines were screened alongside the wildtype control (Bd 21-3) at ambient CO_2 concentration (~ 400 ppm) through thermal imaging. Initial

screening was done in the M5 generation using 5 replicates for each line tested. Lines appearing to be warmer or cooler than the wildtype at ambient CO_2 were retested in the following week as confirmation of phenotype. 50 lines were selected in the initial screen, but after lines were regrown and tested again in the same generation, only 28 displayed consistently changes in the canopy leaf temperature compared to WT. The confirmed 28 lines were then taken into the M6 generation to further characterize the phenotypes observed. Characterization of mutant lines included stomatal development analyses, thermal imaging after 2 hours under high CO_2 conditions, and intact leaf gas exchange. During characterization of these mutant lines in the M6 generation, I joined the team. 12 of the 28 lines that were taken into the M6 generation were confirmed to have lower canopy leaf temperature including mutant lines chill 1, 10, and 15.

Characterization of chill 1 was first pursued through thermal imaging after exposure to high CO_2 for 2 hours as compared to wildtype (Bd 21-3) (Figure 1.1A). Further analysis of the thermal images shows that chill 1(right) is approximated to be at least 1℃ cooler than wildtype (left) after exposure to the same conditions and being of similar size. To see if this phenotype was due to an impairment in stomatal closure, intact leaf gas exchange analysis was performed on both chill 1-like plants and wildtype (Bd 21-3) (Figure 1.1B). Plants were allowed to equilibrate for an hour and were then exposed to low CO_2 (150 ppm) where chill 1 showed a similar stomatal conductance to the wildtype. After an hour and a half plants were switched to high CO_2 (900 ppm) after which a rapid drop in stomatal conductance was observed in wildtype (Bd 21-3); however, stomatal conductance of chill 1 remained steady. Plants were also exposed to ABA (Figure 1.1C) to determine whether the stomata in chill1 were able to close in response to another stimulus. Following equilibration for 1 hour, ABA was added 10 minutes after stomatal conductance

measurements began. After addition of ABA, there was a sharp decline in conductance for both mutant and wildtype lines to below less than half of the original conductance values observed.

Backcrossing of chill 1 to the wildtype (Bd 21-3) was pursued to determine if the mutation was likely to be dominant or recessive as observed in the resulting F1 progeny. Figure 1.2A shows the thermal image comparing the F1 backcross (right) to both parental lines (Bd 21-3 left, chill 1 middle) in which the backcrossed mutant resembles the wildtype. To compare stomatal conductance data between the parental lines, intact leaf gas exchange was performed on chill 1 and wildtype. chill 1 responds in a similar manner to wildtype for both ambient (400 ppm) and low CO_2 (150 ppm) but remains steady under high CO_2 (900 ppm) while wildtype shows a rapid decrease (Figure 1.2B). Stomatal conductance was also measured for the backcross progeny (Figure 1.2C) showing that the backcrossed line shows a wildtype-like phenotype under all CO_2 conditions. To take the backcrossed line into the F2, tillers were created from the F1 plants to ensure enough seeds were obtained. The F1 tiller population of backcrossed lines was grown, from which approximately 6,000 seeds were collected. Estimation of the total amount of seeds was done using the averaged weight of 20 filled seeds. From those seeds, the F2 mapping population was grown, and thermal imaging was conducted to identify mutants that were chill 1 like. Plants were exposed to high CO_2 for 2 hours before imaging was conducted, those appearing cooler than the wildtype (left) in the image were predicted to be chill 1 like (Figure 1.3A). Color images were also taken of the plants during thermal imaging which allowed for identification of individual plants suspected to be chill 1-like after completion of blind thermal imaging analyses by three independent members of the team (Figure 1.3B).

Characterization of chill 15 was pursued in a similar manner beginning with thermal imaging (Figure 1.4A) showing chill 15 also remained cooler than wildtype after exposure to high

CO_2 (900ppm). To determine if the observed difference in canopy leaf temperature could be due to having an increased number of stomata, images were taken under the DIC microscope and stomatal index and density were calculated. Neither stomatal index nor density were shown to be significantly different from wildtype following statistical analysis (Figure 1.4B). Identification of possible stomatal impairment was pursued through stomatal conductance analyses. Under low CO_2 (150 ppm) conditions, chill 15 responds similarly to wildtype. After exposure to high CO_2 (900ppm), a sharp decline in wildtype conductance is observed of almost 40%, whereas conductance measured by chill 15 drops by less than 10% (Figure 1.4C). In a separate experiment, stomatal conductance was measured in the presence of ABA. After allowing plants to equilibrate, ABA was added to both samples. In the presence of ABA, a rapid decline in stomatal conductance can be seen for both wildtype and chill 15, although chill 15 shows a slower decline (Figure 1.4D).

Further characterization of chill 15 included crossing to wildtype, resulting in the F1 progeny to be used to determine if the mutation presented as dominant or recessive. Thermal imaging was pursued for the resulting F1 progeny (Figure 1.5A) showing the backcross (right) in comparison to parental lines (wildtype left, chill 15 middle). As observed in the thermal image, the backcrossed mutant appears to be cooler than the wildtype line after exposure to high CO_2, similarly to the chill 15 mutant line. Intact leaf gas exchange analyses were performed on chill 15 and wildtype lines under ambient (400 ppm), low (150 ppm) and high (900ppm) CO_2. Figure 1.5B shows that under ambient and low CO_2 chill 15 stomatal conductance very closely reflects the conductance values measured by wildtype. Under high CO_2 conditions there is a slower linear response by chill 15 compared to the exponential decline in conductance observed by the wildtype. Stomatal conductance was also measured for the chill 15 backcrossed line compared to wildtype

showing a similar trend. Conductance values were otherwise indistinguishable except under high CO_2, where the mutant line shows a much slower decline in conductance (Figure 1.5 C).

Under normal conditions, stomatal closure induced by stress will not subside until the stress inducing stimuli has been removed. However, preliminary work suggests there may be a mutant that is unable to maintain stomatal closure. Possible stomatal reopening was first identified during intact leaf gas exchange analyses to initially characterize the mutant. Under all CO_2 conditions the mutant line chill 13 responds similarly to wildtype. Under high CO_2 stomatal conductance for both chill 13 and wildtype drops suddenly, but conductance of chill 13 appears to begin increasing again over time (Figure 1.6A). Data was normalized to the first 10 minutes following equilibration and the possible reopening of stomata can still be observed (Figure 1.6B). To observe this over a long period of time thermal imaging was conducted. A high CO_2 (900ppm) time course was performed on chill 13 alongside wildtype over the course of 6 hours observed through thermal imaging (Figure 1.7). Images were taken at ambient CO_2 for which there are no distinguishable differences between mutant and wildtype temperature. Plants remain a similar temperature through hours 0-3. As observed in the remaining 3 hours of the time course, chill 13 appears to become cooler than the wildtype line which may be indicative of stomatal reopening, even under high CO_2.

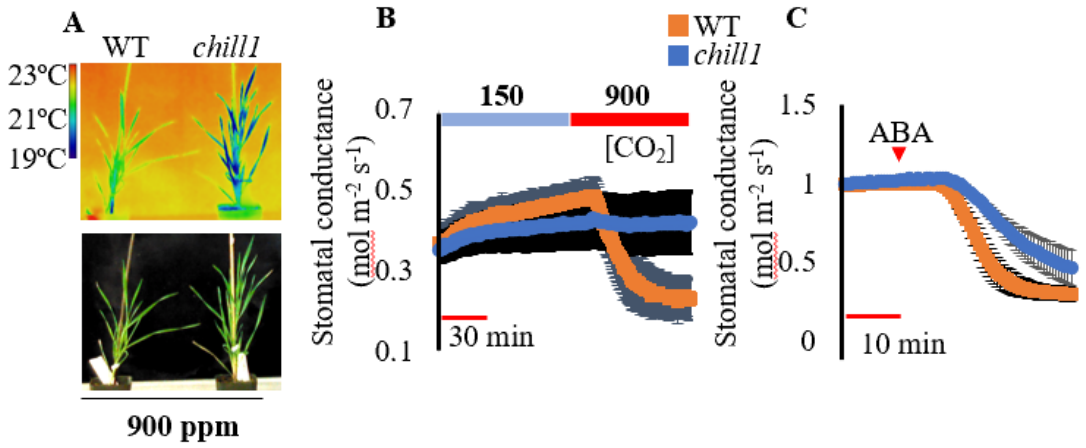

Figure 1.1*:* Characterization of the Chill 1 mutant line. Experiments conducted by Dr. Paulo H. O. Ceciliato.

(A) Thermal imaging was done on four-week old plant after exposure to high [CO_2] (900 ppm) for 2 hours. Plants were imaged utilizing infra-red thermal imaging camera within 30 seconds after removal from the hgh CO_2 growth chamber. Bd 21-3 (wildtype) left, and chill 1 mutant line right. (B) Stomatal conductance of Bd 21-3 (WT) and chill 1 mutant line was analyzed with a gas exchange analyzer through n=3 experiments $\pm$ SEM, using 4 leaves per experiment, 12 leaves per genotype in total. (C) Stomatal conductance in the presence of 2 μM ABA added to the transpiration stream of the intact leaves (arrowhead). Data was normalized to conductance pre-ABA (data obtained from n=3 experiments $\pm$ SEM, using 4 leaves per experiment, 12 leaves per genotype total).

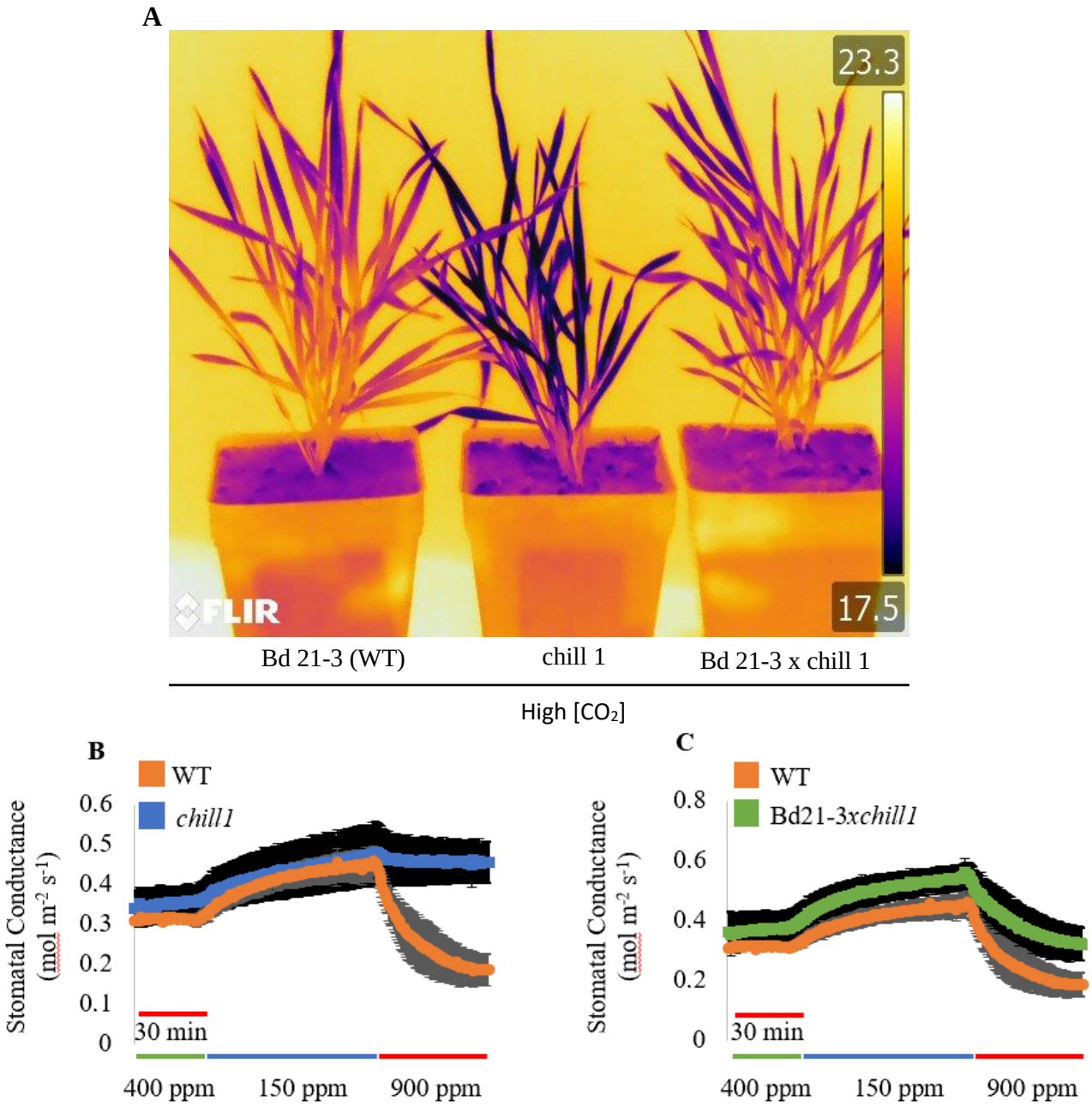

Figure 1.2: Characterization of Bd 21-3 x chill 1 backcross.

Thermal imaging was conducted on tillers created from parental lines and F1 backcrosses (A). Plants are arranged left to right: Bd 21-3 (wildtype), Chill1, Chill 1 x Bd 21-3. Image was taken after exposure to high CO_2 (1000 ppm) for 3 hours. Plants were the same age and grown in parallel. (B) Stomatal conductance of Bd 21-3 (wildtype) and *chill 1* mutants grown in parallel analyzed using a gas exchange analyzer. Data presented are the average of n=3 experiments $\pm$ SEM, 4 leaves were used per experiment, 12 leaves per genotype total. (C) Stomatal conductance of Bd 21-3 (wildtype) and Bd 21-3 x *chill 1* mutants grown in parallel analyzed using a gas exchange analyzer. Data presented are the average of n=3 experiments $\pm$ SEM, 4 leaves were used per experiment, 12 leaves per genotype total.

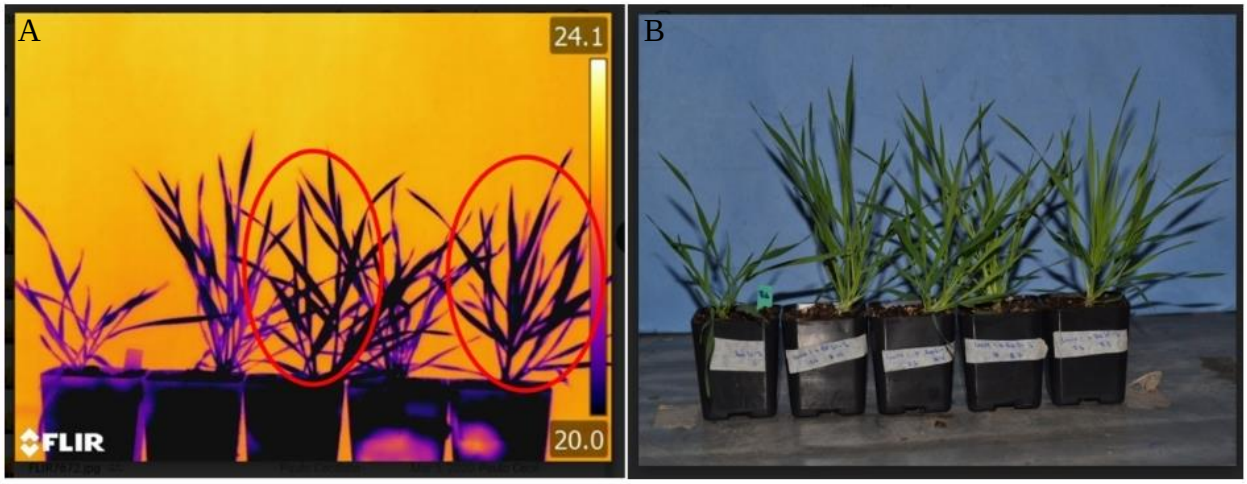

Figure 1.3: Thermal imaging screen of chill 1 x Bd 21-3 backcross in F2.

Thermal imaging was conducted on the F2 mapping population of chill 1 x Bd 21-3 backcrosses after exposure to high CO_2 (900 ppm) for 2 hours (A). The F2 population of plants contained approximately 580 plants imaged alongside the wildtype control Bd 21-3 (left). Color images of the same plant pairs were taken simultaneously on the same camera for individual plant identification (B).

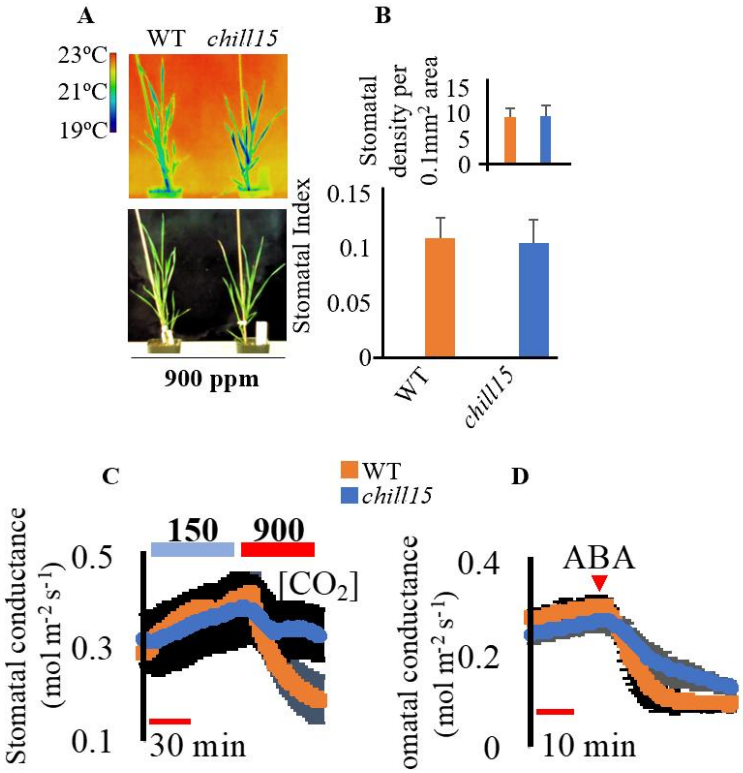

Figure 1.4: Characterization of Chill 15. Experiments conducted by Dr. Paulo H. O. Ceciliato.

(A) Thermal imaging was done on four to five-week old plant after exposure to high [CO_2] (900 ppm). Plants were imaged utilizing infra-red thermal imaging camera within 30 seconds after removal from the hgh CO_2 growth chamber. Bd 21-3 (wildtype) left, and *chill 15* mutant line right. (B) Stomatal index and density was calculated using 4 images per leaf with 5 leaves per genotype on five week old plants. (C)Stomatal conductance of Bd 21-3 (WT) and chill 1 mutant line was analyzed with a gas exchange analyzer through n=3 experiments $\pm$ SEM, using 4 leaves per experiment, 12 leaves per genotype in total. (D) Stomatal conductance in the presence of 2 μM ABA added to the transpiration stream of the intact leaves (arrowhead). Data was normalized to conductance pre-ABA (data obtained from n=3 experiments $\pm$ SEM, using 4 leaves per experiment, 12 leaves per genotype total).

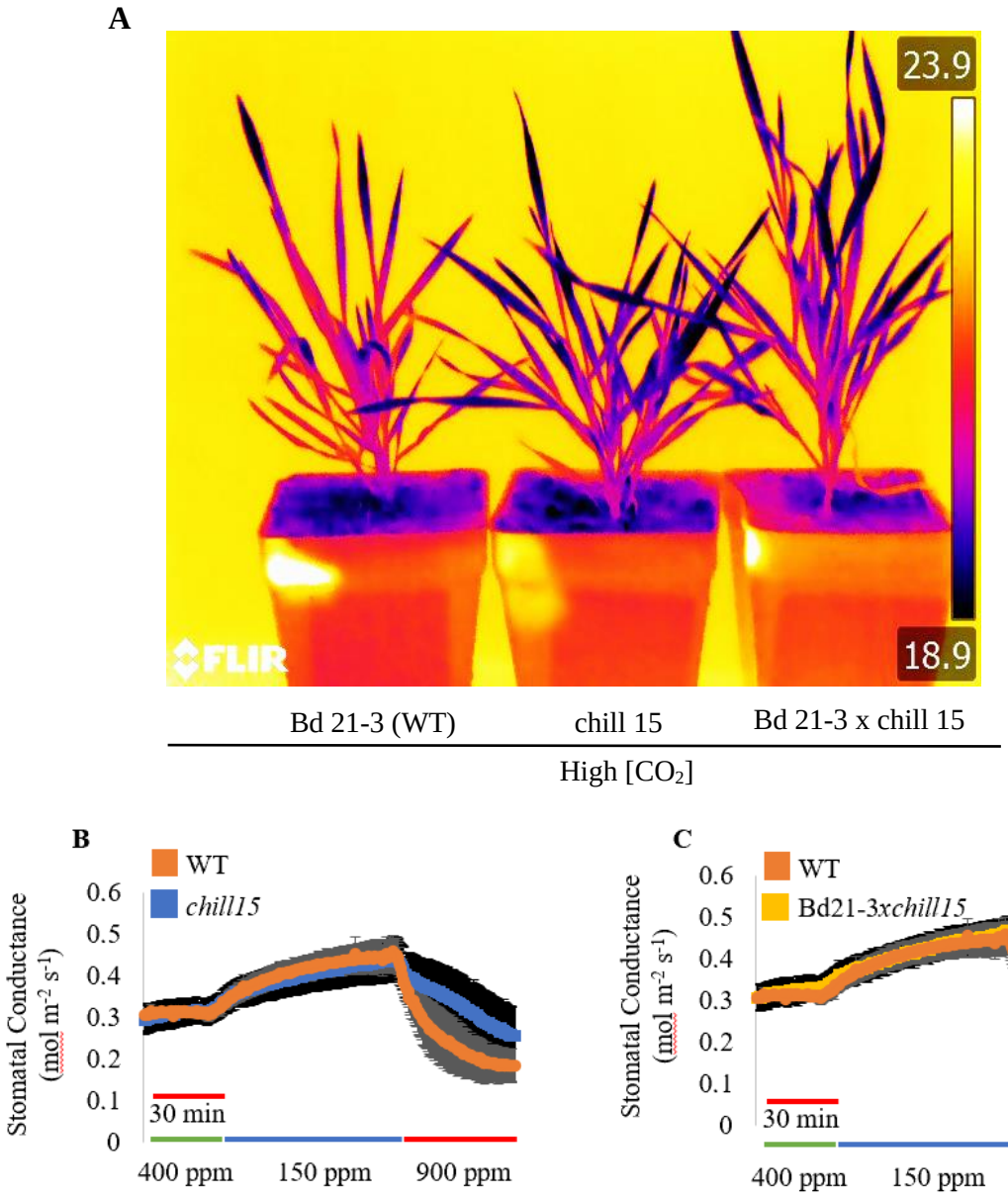

Figure 1.5: Characterization of Bd 21-3 x Chill 15 backcrosses. Gas exchange conducted by Dr. Paulo H. O. Ceciliato.

Thermal imaging was conducted on tillers created from parental lines and F1 backcrosses. Plants are arranged from left to right, Bd 21-3 (wildtype), Chill 15, Chill x Bd 21-3 (A). Image was taken after exposure to high CO_2 (1000 ppm) for 3 hours. Analyses were done on plants of the same age grown in parallel. (B) Stomatal conductance of Bd 21-3 (wildtype) and *chill 15* mutants grown in parallel analyzed using a gas exchange analyzer. Data presented are the average of n=3 experiments $\pm$ SEM, 4 leaves were used per experiment, 12 leaves per genotype total. (C) Stomatal conductance of Bd 21-3 (wildtype) and Bd 21-3 x *chill 15* mutants grown in parallel analyzed using a gas exchange analyzer. Data presented are the average of n=3 experiments $\pm$ SEM, 4 leaves were used per experiment, 12 leaves per genotype total.

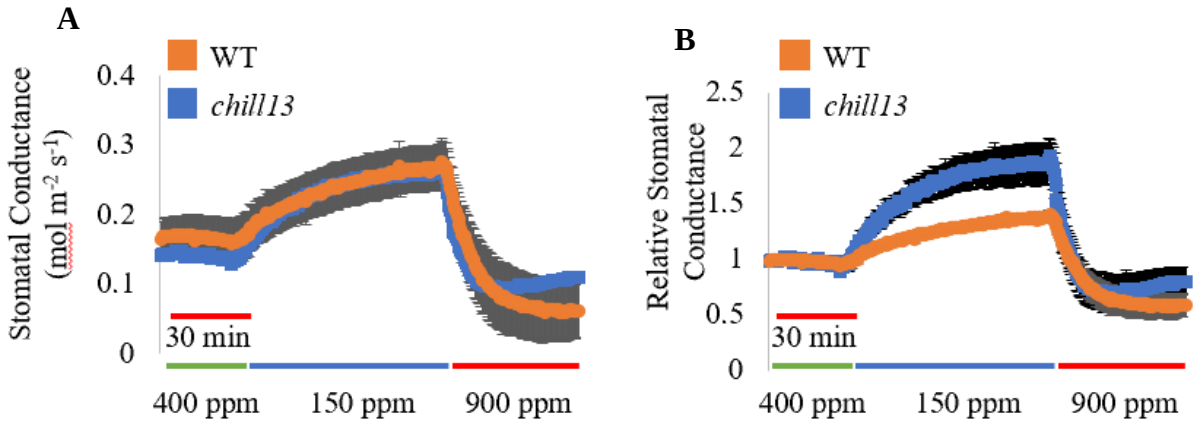

Figure 1.6: Responses to [CO_2]-shifts in chill 13. Gas exchange conducted by Dr. Paulo H. O. Ceciliato.

The stomatal conductance (gs) of Bd 21-3 (wildtype) and *Brachypodium distachyon* mutant *chill* 13 leaves were analyzed using a gas exchange analyzer. Data was gathered through n ≥ 3 ±SEM experiments, utilizing four leaves per experiment (minimum 12 leaves per genotype). Data from the left graph (A) was normalized to the average conductance observed in the first 10 minutes (B).

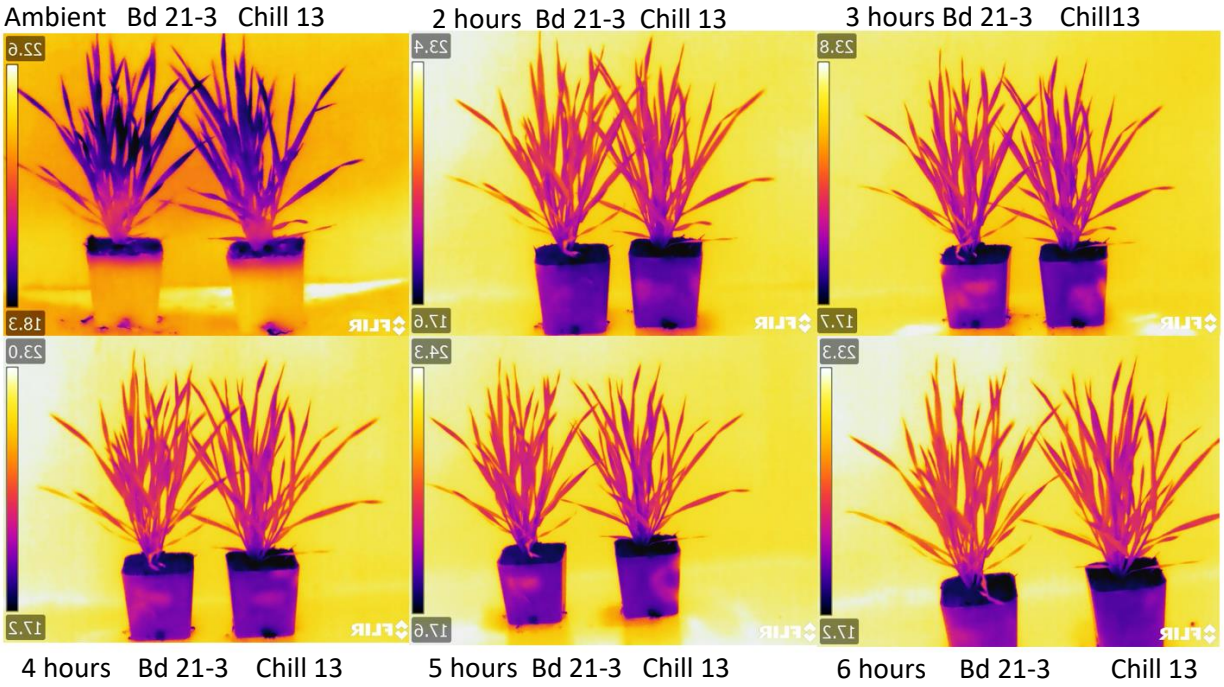

Figure 1.7: Thermal imaging time course of Chill 13 and Bd 21-3 (WT).

Thermal imaging was conducted on pairs of Chill 13 mutant lines alongside Bd 21-3 (wildtype) under high [CO_2] of 900 ppm over the course of 6 hours. Plants were imaged at ambient CO_2 followed by time points 2-6 in the same respective pairs.

1.2.2 Crossing Brachypodium distachyon

Following phenotypic characterization of chill mutant lines, crossing was pursued to better understand the nature of the mutation. Crossing also allows for testing possible allelic relationships between mutants, assessed through crossing different chill lines. Backcrossing mutants is the process of crossing the mutant line of interest to the wildtype (Bd 21-3). Through this process, the F1 generation is utilized to observe if the mutant is likely to be dominant or recessive based on the

phenotype present. By allowing the F1generation to self-cross, the F2 mapping population is generated. The process of crossing was carried out over the span of 2 days as outlined by Michael Steinwand and John Vogel (Steinwand & Vogel, 2010). Day 1 of the crossing procedure involves emasculating the plant that is going to be used as the "mother", the plant that will be pollinated and will grow the seed following successful crossing. The process of emasculation involves removing the anthers from a healthy plant containing a fully developed stigma but immature anthers that have not yet released pollen. Anthers are removed using fine tipped forceps without disturbing the stigma at the base of the flower (Figure 1.8). On Day 2 an older plant of the other line of interest for the cross is selected. The mature anthers are removed from the plant and placed onto a slide allowing pollen to be visualized for those that dehisce. Anthers that dehisce on the slide without being ruptured were selected and were lightly applied to a healthy stigma that was emasculated the previous day (Figure 1.9).

Optimization of *Brachypodium distachyon* crossing techniques were required as initial crossing procedure showed very limited success rates. Both growth conditions and crossing technique were altered, appearing to have been very effective in circumventing issues with unhealthy plants and immature pollen. Plants were initially grown under insufficient light conditions and became etiolated. To produce healthier plants, they were exposed to higher light intensity, closer proximity to the source, and regular measurements of light intensity. Perlite and vermiculite were also added to soil before potting, and fertilization solution (1X) was utilized when watering plants. All of these conditions yielded higher quality plants which also grew healthier flowers to be used for crossing. Optimization of the crossing protocol was done through analysis of combined failures. Even in flowers containing a healthy stigma on day 2, if the lemma had been pulled too far back, the flower would not close properly even if held closed with Parafilm. It was

initially proposed that flowers that would not close properly without assistance could be taped shut, though it has not shown very high efficiency as closing the flowers with too much force appears to also be able to damage the stigma. It has been hypothesized that flowers which have been opened too far in either step of crossing and cannot remain closed on their own will not yield successful crosses, even if taped. Selection of anthers was also difficult, as anthers must be harvested the same day, and applied very gently to the stigma without ever making direct contact. It was originally suggested that both yellow and white anthers could effectively be used in crossing while green should be dismissed as immature. Although, there has been little success with white anthers as well, and they appear to be unable to dehisce, or will not do so to the extent that yellow anthers are capable. Therefore it is suggested that only anthers with yellow stigma that dehisce within 10 minutes after harvesting should be used for the purposes of crossing.

Several lines have been crossed using the above outlined method of crossing including backcrossing of chill lines 1, 10, and 15, along with crossing chill lines 1 and 15 while others remain in progress (Figure 1.10). Many of the crosses were worked on alongside Li Zhang, who completed much of the preliminary backcrossing (Table 1). Efforts to backcross the remaining most promising chill mutants is still underway and will be pursued following her advice.

In Brachypodium, only one seed is generated from a successful cross, as such completing one cross will not yield enough seeds to result in a sizeable mapping population. To solve this problem tillers, or cuts, can be made from plants to increase the amount of plants in a given population. Seeds resulting from the F1 crosses have been grown under short day allowing the plants to become very large. As *Brachypodium distachyon* becomes very large aerial roots will begin to form at nodes which can then be cut and placed into water for a minimum of 7 days. While submerged new roots will begin to grow and after being transferred to a pot the cut will become

its own plant. Generation of the tiller population outlined in Figure 1.11 allowed for enough seeds to be collected from the F1 generation to pursue mapping in the following generation. Large numbers of tillers were created for backcrosses for chill mutants 1, 10, and 15. Due to the size and volume of the tillers thousands of seeds were grown and collected to be used for mutant mapping (Figure 1.12).

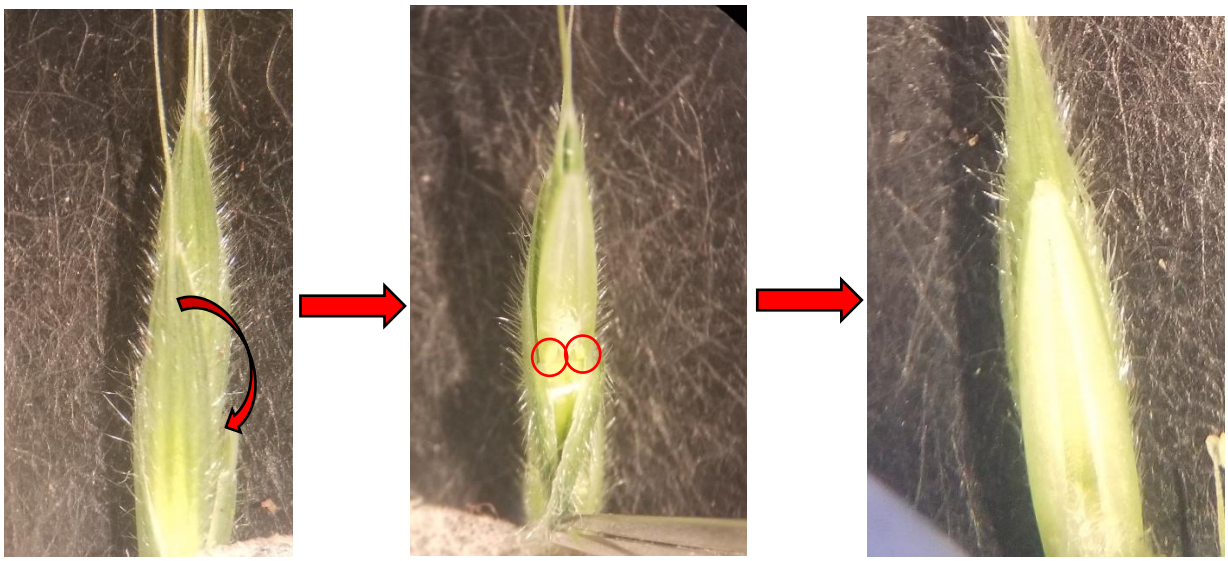

Figure 1.8: Crossing Brachypodium distachyon Day 1, Emasculation

A healthy flower is selected for emasculation. The lemma is peeled back without opening the flower all the way causing stigma damage. Utilizing fine tipped forceps, anthers can be removed unless they are at the level of or higher than the stigma. Special care must be taken to prevent causing damage to the stigma. Following emasculation, the lemma can be replaced recovering the stigma.

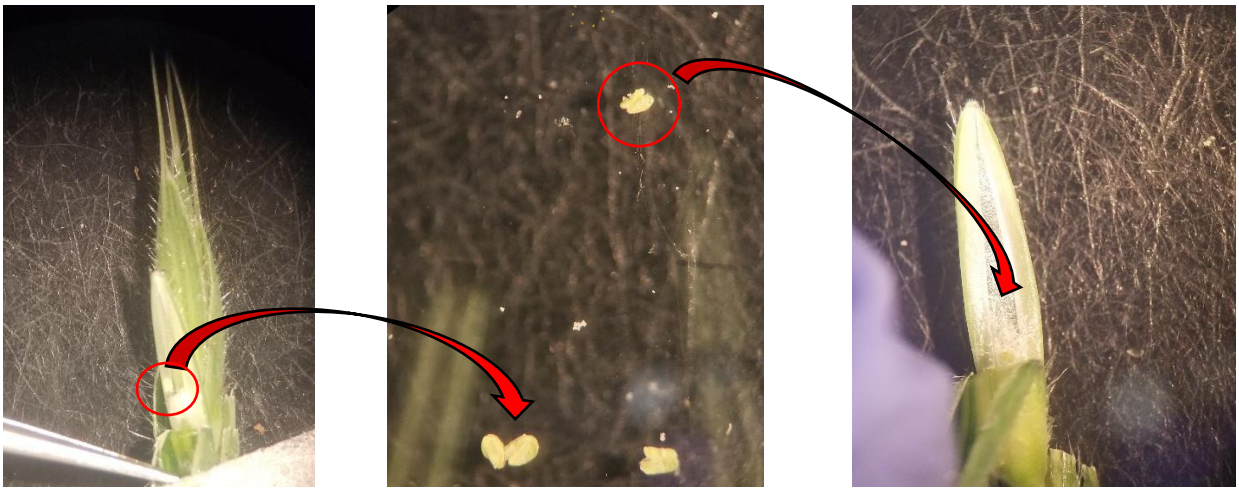

Figure 1.9:Crossing Brachypodium distachyon Day 2. Pollination

The following day anthers can be harvested from a plant with mature (yellow or white) anthers that have begun to grow upwards of the stigma structure. Stigma removed are placed onto a slide and allowed to dehisce. Only those that dehisce on their own for which pollen can be visualized under the microscope are selected. Anthers are then applied to the emasculated plants from the previous day only if the stigma has not sustained damage. Following pollination, the flower can be taped shut if it will not close. Successful crosses can be visualized within a few days as the seed begins to develop.

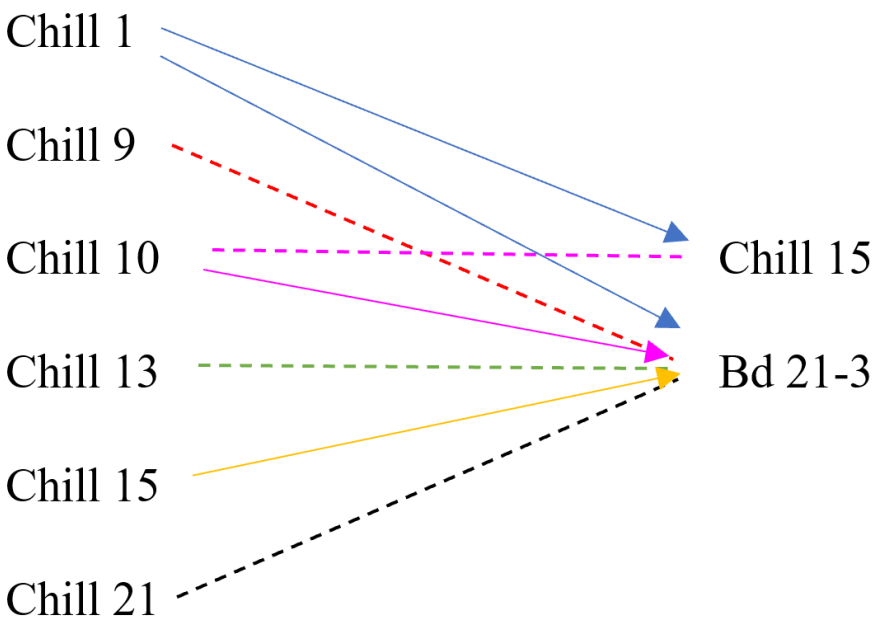

Figure 1.10: Visual representation of planned, executed and on-going crosses

Arrows correspond to crosses that have either been completed, are currently being pursued or have been planned. Back crossing to Bd 21-3 (wildtype) has begun or been planned for all lines. Solid lines indicate crosses that have been completed. Dashed lines indicate crosses that are currently being pursued or are planned.

Table 1: Status of crosses for EMS lines

Crosses presented in this table are those that have been completed or are undergoing or planned. Backcrosses for Chill 1, 10, and 15 have been pursued but were completed by Li Zhang (L.Z.) for which the number of seeds resulting from successful crosses has been estimated.

Cross	Status	Crosses completed	Seeds
Chill 1 x Bd 21-3	F2 is growing	Crossed by L.Z.	5 (4 germinated)
Chill 10 x Bd 21-3	Tillers are growing	Crossed by L.Z.	6 (6 germinated)
Chill 15 x Bd 21-3	F2 is growing	Crossed by L.Z.	10 (9 germinated)
Chill 1 x Chill 15	Growing	Crossed by L.Z.	5 (4 germinated)
Chill 9 x Bd 21-3	Ongoing	N/A	N/A
Chill 10 x Chill 15	Ongoing	N/A	N/A
Chill 13 x Bd 21-3	Ongoing	N/A	N/A
Chill 21 x Bd 21-3	Ongoing	N/A	N/A

Seeds harvested from successful crosses were cold treated for a minimum of 7 days

↓

After being transferred to soil plants were grown under short day conditions (6 light: 18 dark) to prevent flowering and promote large growth.

↓

Cuts were made under nodes after initial growth of aerial roots.

↓

Cuts were placed into tubes containing 1% fertilizer for a minimum of 1 week.

↓

Plants were transferred to soil following root growth and allowed to establish before switching to long days (22 light: 2 dark) promoting flowering.

Figure 1.11: Generation of the tiller population

After successfully crossing lines tillers can be created from the mother plant to allow for a larger F1 generation to facilitate mapping of the mutant gene. Short day inhibits flowering in *Brachypodium distachyon* leading to large plants. Tillers were made from cuts below the node from which aerial root have formed. Cuts were placed into fertilizer containing solution and allowed to grow before transfer to soil. Following root establishment in soil plants were switched to long day (22light : 2 dark) to promote flowering.

Genotype of cross	Number of tillers created	Total seed collection
Chill 1 x Bd 21-3	31	Approximately 6,000
Chill 10 x Bd 21-3	8	Approximately 1,200
Chill 15 x Bd 21-3	34	Approximately 6,300

Figure 1.12: Number of seeds collected from tiller population

Generation of the tiller population led to a large number of seeds after plants were switched to long days to promote flowering. Estimations were done by creating a standard weight of 20 individual seeds predicted to be viable.

1.3 Discussion:

The first forward genetic screen of EMS mutagenized *Brachypodium distachyon* was initiated to identify individual mutants that could be impacted in CO_2 response, as observed through thermal imaging. Forward, or classical, screens such as this have been predicted to have great potential in identification of unexpected contributors to a given phenotype (Marriott et al., 2014). As the CO_2 signaling pathway has been extensively studied and characterized in other model organisms, but not in grasses, a forward genetic screen was useful in possible determination of genes not previously implicated in this pathway, or that contribute in a different manner.

Throughout the screen 1075 independent mutagenized lines in the M5 generation were screened, and 50 lines were selected to have shown altered canopy leaf temperature when compared to the wildtype control (Bd 21-3). Upon completion of the initial screen, it was noted that plants may not have been grown under optimized growth conditions. To combat this, growth conditions were adjusted, and the 50 lines selected in the initial screen were screened again in the M5 generation, resulting in 28 mutants that were shown to be colder than wildtype. The 28 mutants that were identified in the secondary screen were taken into the M6 generation for a tertiary screen and further characterization of mutant lines.

The tertiary screen of the remaining 28 mutant lines was done under high CO_2 (900 ppm), to identify those that may be impaired in stomatal response. Thermal imaging was utilized for this process as plants that are impaired in stomatal closure in response to high CO_2 will appear cooler as evapotranspiration has not been inhibited by stomatal closure (Engineer et al., 2014). The first 7 lines screened were not shown to have reproducible phenotypes, appearing wildtype-like in M6, and were then excluded. The remaining 21 lines that had not yet been confirmed in M6 were kept as the ‘chill mutants’, numbered 1-21. Lines were analyzed using tertiary thermal imaging

analyses, along with stomatal index and density calculations, and intact leaf gas exchange analyses. While some of the *chill* lines were classified as wildtype-like following characterization in M6; several were shown to display robust phenotypes that were reproducible and distinct from the wildtype control.

During preliminary characterization of *chill* mutant lines, stomatal index and density was measured for all 21 lines. This was done to determine if the mutations sustained leading to cooler canopy leaf temperature could have been a result of a plant containing more, or larger stomata on the leaf surfaces. A plant containing larger or higher numbers of stomata would potentially be able to do more gas exchange through their stomatal pores, allowing for higher rates of evapotranspiration, and therefore lower canopy leaf temperature (Engineer et al., 2014; Vráblová et al., 2017). However, following stomatal imaging analyses, all 21 lines were shown to contain wildtype-like development of stomata, suggesting that the phenotype is likely due to stomatal movement; not development. Currently stomatal pore length, aperture, nor subsidiary cell size have been measured, which if drastically different from wildtype could contribute to a cooler phenotype.

Some of the mutants characterized in M6 include a subgroup that appear to show strongly impaired stomatal closure under high CO_2, but no such impairment can be observed when plants are exposed to exogenous ABA during intact leaf gas exchange analyses. This subgroup includes *chill 1*, *chill 15*, *chill 20*¸ and potentially *chill 10*; however, further experimentation will be required.

Mutants of similar phenotypes have been observed in *Arabidopsis thaliana*, which is a much more extensively studied model organism. Due to the similarity of the recorded phenotypes of mutants in *Arabidopsis* to some of the mutants observed, it was hypothesized that at least one

of the chill lines may be a similar mutation in *Brachypodium*. Mutations that also show inhibited stomatal closure under high CO_2 but that will be respond to ABA include *SLAC1* which would be activated under both high CO_2 and ABA, *HT1* or *OST1* both of which are upstream of *SLAC1* and transduce signals downstream to open the anion channel (Hiyama et al., 2017). *MPK4/12* have also been shown to contribute meaningfully to this pathway by upregulating *HT1* when active, therefore loss could potentially also show inhibited stomatal closure in response to high CO_2 (Hiyama et al., 2017).

It has been shown in previous studies that *MPK12* functions upstream and possibly in an epistatic manner to *HT1*, leading to specific inhibition of *HT1* (Jakobson et al., 2016). Characterization of *mpk12* mutants were shown to be unable to inhibit *HT1*, which lead to stomata that appeared to be more open even in the presence of high CO_2. *mpk12* also displayed wildtype-like responses when exposed to ABA (Jakobson et al., 2016). More open stomata under ambient and high CO_2 lead to higher stomatal conductance as was observed with *chill 1* and *15*. The same study proposes that since both *MPK4* and *MPK12* are very closely related, both may contribute to CO_2 responses, which was confirmed through Y2H (Yeast two-hybrid) experiments (Jakobson et al., 2016).

Similar to the manner in which *mpk4/12* mutants show observable impairments in stomatal closing in response to fluctuations in CO_2 concentrations, but appear to have wildtype-like ABA functionality is *βca4* (Hu et al., 2010). It has been noted that increased intracellular concentrations of both CO_2 and bicarbonate are required for activation of *SLAC1*. Therefore, if the reaction converting CO_2 into bicarbonate cannot be completed, this may be the reason this phenotype is observed (Hu et al., 2010).

Downstream of *MPK4/12* are *HT1 and* OST1. There are 2 known mutant lines for *HT1*, including *ht1-1* and *ht1-2* both of which showed reduced response to CO_2 changes, or in the case of *ht1-2*¸almost no difference in leaf temperature in response to altered CO_2 concentrations could be observed (Hashimoto et al., 2006). While chill lines 1, 10, and 15 all display cooler leaf temperature under ambient and high CO_2, a possible mutation in *HT1* was not excluded from possible list of candidate genes. *ht1* is also one of the few mutations known within the CO_2 signaling pathway known to be a dominant mutation and has been shown to display constitutively higher stomatal conductance (Hõrak et al., 2016). It has been proposed that this may be a potential candidate gene to explain the phenotype observed in *chill 15*. Based on thermal imaging and intact leaf gas exchange data obtained from the F1 backcrossed population, *chill 15* may be at least semi-dominant, as the entire population appeared to be *chill 15*-like under all conditions.

Whereas *ost1* mutant lines display a less similar phenotype to the observed phenotype of the *chill* mutant lines. It was originally hypothesized that *OST1* did not contribute to the CO_2 signaling pathway; however, this has shown to be untrue, and mutants have been shown to be impaired in both high CO_2 and ABA responses (Xue et al., 2011). Due to the robust impairment in CO_2 response in *ost1*, it has remained a possible candidate gene in *chill* mutants, although they do not display impairments in ABA responses. As *OST1* is crucial for ABA signaling (Xue et al., 2011), it is not expected to be the causative mutation, but due to the lack of characterization in *Brachypodium distachyon*, it has not been excluded as a possibility.

Anion channels such as *SLAC1* have been regarded as critical processes involved in stomatal closure (Schroeder & Hagiwara, 1989). Mutations in this gene lead to greatly reduced functionality of anion channels, leading to an increase of anions present within the guard cell protoplasts, affecting the osmoregulation utilized to control stomatal aperture (Negi et al., 2008).

Altered distribution of these osmolarity regulating anions has strong negative affect on the plants ability to control stomatal movement in response to CO_2. However, ABA activated channels and physiological responses were shown to remain intact, even in *slac1* lines displaying greatly reduced CO_2 responses (Xue et al., 2011; Zhang et al., 2018).

Further characterization of *chill* lines was done with the aim of mapping causative mutations for lines 1, 10 and 15. This was done through backcrossing the mutant lines confirmed to show their respective *chill* phenotypes through thermal imaging prior to crossing. Lines were crossed to wildtype (Bd 21-3) to reduce the possible number of passenger mutations potentially contributing to the observed phenotype, and to determine if the causative mutation appeared to be dominant or recessive. Crossing was done according to the Steinwand and Vogel method over the course of 2 days utilizing forceps and a dissection microscope (Steinwand & Vogel, 2010).

F1 populations have been obtained for both *chill 1* and *chill 15* backcrosses. The F1 population for the *chill 1* backcross appeared to be wildtype-like following thermal imaging under high CO_2, and intact leaf gas exchange (Figure 1.2). Whereas the F1 population for the *chill 15* backcrossed population was observed to be at least semi-dominant, as the F1 displayed a *chill 15*-like phenotype in both thermal imaging under high CO_2 and intact leaf gas exchange (Figure 1.5).

The intention in backcrossing was to create a population to be used to map the causative mutation. As the F1 population was very small due to only a single seed obtained per successful cross, Dr. Daniel Woods was contacted about how to bulk the F1 generation. His recommendation was to create a population of tillers, cut from successful crosses in the F1 generation grown under short day (8 hours light/16 hours dark) promoting large growth. Once *Brachypodium* gets very large, branches will begin to form aerial roots at nodes. By cutting below the node growing aerial roots, cuts can be grown up alongside the mother F1 plants to increase the size of the population

without having to obtain further crosses. Following the advice of Dr. Daniel Woods, sizeable F1 populations were obtained for both the *chill 1* and *chill 15* backcrosses.

Following bulking of the F1 generation, a large number of seeds was obtained to generate the F2 population. Approximately 588 F2 *chill 1* backcrossed plants were grown up, once large enough, thermal imaging was conducted on plants in staggered batches after exposure to high CO_2 for 2 hours. Thermal imaging was conducted to identify plants displaying a *chill 1*-like phenotype, as it was predicted to be recessive based on the F1 thermal imaging screen. Initial thermal imaging conducted on the F2 mapping population identified 116 plants appearing cooler under high CO_2, indicative of the *chill 1* phenotype. DNA was extracted from all lines identified as being *chill1*-like, along with wildtype to be used as a control for sequencing.

Sequencing was done to be done on DNA extracted from the F2 population utilizing WGS (Whole Genome Sequencing) along with BSA (Bulked Segregant Analysis). Therefore, in an effort to reduce noise within the sample population sent for sequencing, and prevent false positives within the population, thermal imaging data was re-analyzed in a blind manner. This was completed another teammate who had not previously seen the thermal imaging data, nor the compiled list. The list contained all lines previously identified as *chill1*-like appearing to be colder when compared to the wildtype control that was present in every image. Secondary thermal imaging analyses were done on the entire population of images with no indication of plants that had been selected as mutant or wildtype. The secondary thermal imaging analyses were done in rounds, the first of which was identification of all *chill 1*-like plants, similar to the initial screen. However, the secondary screen was followed up by several subsequent rounds of elimination, leading to formation of 3 groups of mutant plants in the F2 generation. The first group contained plants that appeared to show the mutant phenotype, but in a weaker manner, leading to exclusion

from the population utilized in WGS and BSA. The second group consisted of 57 plants to be used for WGS that displayed the mutant phenotype clearly. The third group was a subset of group 2 and contained the 25 lines with the strongest phenotype as observed in the images.

Following the formation of the groups classifying the strength of the mutant phenotype, final results were compared to results from the initial screen, and DNA from the indicated plants were pooled to be sent for WGS and BSA. This method was utilized to allow for generation of a sequencing library to identify the causative mutation that is recurring among the lines displaying the mutant phenotype. BSA is also very useful as it allows for some mistakes in phenotyping due to the robustness of the analysis (Schneeberger et al., 2009). Identification of a mutated gene shared by all lines displaying the mutant phenotype will allow for determination of the causative mutation.

Another line that appeared to be interesting after initial characterization was *chill 13*. Initially *chill 13* was thought to show potential stomatal reopening based on preliminary thermal imaging and intact leaf gas exchange analyses (Figures 1.6 and 1.7). It was observed that although stomata appeared to respond similarly to wildtype to high CO_2, stomata did not appear to remain closed after extended periods of time under stress. It was observed during intact leaf gas exchange that after exposure to high CO_2, stomatal conductance would drop at almost the same rate as the wildtype control, but appeared to show an increase in conductance shortly after which was not observed in wildtype. Plants were also grown alongside wildtype plants, and both were exposed to high CO_2 during a time course through which they were imaging utilizing the thermal imaging camera. It was observed during this that after about 3 hours, chill 13 appeared cooler than wildtype, further supporting the idea that stomata may be reopening.

A possible explanation for this was originally hypothesized to be that perhaps *chill 13* contained less ABA even at a basal level, which was inhibiting stomata from remaining closed for

extended periods of time. It has been shown by previous studies that some mutants sustained within the ABA pathway would respond similarly to wildtype under high CO_2 and would close rapidly, but could not maintain closure and stomatal conductance would slowly increase over time (Hsu et al, 2018). This study provided further evidence that the ABA and CO_2 signaling pathways work in tandem, and that ABA may be required to maintain a lowered stomatal conductance under increased CO_2 (Hsu et al., 2018).

Another explanation that was considered to explain the phenotype observed in *chill 13* was a thinner cuticle present on the surface of leaves. One of the major functions of the cuticle is to prevent water loss not regulated through stomatal pores, however, the specific chemical makeup varies between plant species, ecotype, even developmental stage (Qiao et al., 2020). The thickness of the cuticle has been shown to be less important than the composition in promoting water impermeability and plays a large part in drought tolerance (Qiao et al., 2020). Using this information, it was extrapolated that perhaps this may play a role in *chill 13* appearing cooler over time under high CO_2 conditions. However, this may be less likely due to the fact that plants would likely appear cooler consistently due to higher amounts of water loss, not only when exposed high CO_2.

While *chill 13* appears to be interesting and may display distinct stomatal response kinetics when under high CO_2, due to the phenotype not being as robust as some of the other *chill* lines; experimentation on this line has been temporarily halted. *chill 13* also displays very early flowering time, on average approximately 10 days before wildtype, which has made it very difficult to backcross. Further experimentation may be pursued at a later date.

Identification of causative mutations in *chill* lines appearing to be less sensitive to CO_2 could allow for generation of crops less impacted by increasing atmospheric concentrations.

Elucidation of those genes contributing to the CO_2 signaling pathway may be used to generate plants with increased regulation of stomatal movement, or improved water use efficiency which may be crucial for agriculture in the face of worsening climate change (Dettinger et al., 2015).

1.4 Methods:

1. Growth conditions
2. Infra-red Thermal Imaging Analyses
3. Licor Gas Exchange
4. Crossing
5. Generation of Tillers & Growth conditions

1.4.1 Plant Growth conditions:

The M5 and M6 generations of Ethyl methyl sulfonate (EMS) mutagenized lines selected from the previous screen of the seed library obtained from the Joint Genome Institute (JGI) were grown alongside Bd 21-3 (wildtype). All seeds were cold treated at 4℃ for a minimum of 7 days prior to planting. Soil contained a 1:1 mixture of perlite: vermiculite allowing for increased water retention of soil. Plants were grown individually in small pots following germination. Domes were removed from trays 7 days following emergence of the first leaf. Plants were grown under 16-hour light/8-hour dark conditions under 250 $\mu E\ m^{-2}\ s^{-1}$ minimum light intensity which was shown to improve growth conditions. Plants were given 1L water and 2X fertilizer containing solution every other day. Sequence indexed sodium azide (NaN) mutagenized lines predicted to have impactful mutations were grown under the same conditions and were also grown alongside wildtype (Bd 21-3) plants.

1.4.2 Infra-red Thermal Imaging Analyses:

Thermal imaging was conducted on 4-5 week old plants using an infra-red FLIR Thermal Imaging camera T650sc (FLIR Systems, Inc. Wilsonville, OR 97070 USA). Ambient CO_2 imaging

was performed within the growth room at approximately 450 ppm CO_2. High CO_2 thermal imaging was conducted by placing plants within Percival, E-36HO high CO_2 chambers. Images were taken after a minimum of 2-hour exposure to 900 ppm or 1000 ppm CO_2. Imaging following high CO_2 exposure was performed immediately after removal from the chamber before equilibration to ambient CO_2. Plants were removed from the chamber in staggered batches of 2-4 plants and arranged side by side in groups containing both EMS mutagenized plants and wildtype (Bd 21-3) for comparative analysis. Images were analyzed by at least 2 people individually to determine which plants were cooler under ambient and high CO_2 conditions. Plants selected as colder by both were used for further experimentation. Plants from mutagenized lines and wildtype (Bd 21-3) were grown in parallel under the same conditions.

1.4.3 Licor Gas Exchange:

Healthy plants of 5-6 weeks old were selected for gas exchange measuring stomatal conductance (gs) using a Licor gas exchange analyzer (LI-6800, LI-COR, Lincoln, NE, USA). To increase the leaf area to be analyzed, 4 healthy leaves were bound together using micropore tape (3M) without causing damage, and the abaxial side downwards (Ceciliato et al., 2019). Once secured within the machine leaves equilibrated for 1 hour under ambient CO_2 of 400 ppm, 65% humidity, and light intensity of 250 μmol m^{-2} s^{-1}. Measurements were done using a normalized steady state stomatal conductance reading at 400 ppm. Above data are representative of average normalized data from a minimum of 3 experiments each using 4 leaves per experiment (minimum total =12 leaves per genotype).

1.4.4 Brachypodium distachyon Crossing:

Crossing EMS lines was done over the course of 2 days. The oldest spikelet on the youngest inflorescence from healthy plants containing a developed stigma but immature anthers were selected for emasculation. Flowers were taped to the dissection microscope utilizing micropore tape (3M) at the base of the flower. Both anthers were removed using fine pointed forceps without damaging stigma or rupturing anthers and distributing pollen. Following emasculation all other flowers from the inflorescence were removed. Emasculated flowers containing healthy undamaged stigma the following day were pollinated with anthers which were harvested and allowed to dehisce. Extracted anthers were placed onto slides for approximately 20 minutes, those that did not dehisce without using a needle to rupture the anther were not used. Only pollen from anthers which were able to dehisce and for which pollen be visualized under the dissection scope were used. After crossing mother plants were kept in the growth room under well-watered conditions. Successful crosses could be seen within 4 days as seed development began.

1.4.5 Generation of Tillers & Growth conditions:

EMS mutagenized lines were back crossed to Bd 21-3 (wildtype), resulting F1 progeny were grown under short day (8 hours light/16 hours dark) under atmospheric CO_2 conditions. Tillers were cut from healthy plants after aerial root formation. Tillers were cut below the node from which roots grew using a razor blade. They were immediately placed into Falcon Tubes containing a 1X fertilizer solution for a minimum of 7 days. Cuts were transferred to soil and grown under short days (8 hours light/ 16 hours dark) and remained covered with domes for approximately 2 weeks before domes were removed and light conditions were adjusted to long day (22 hours light/2 hours dark) to promote flowering. F1 tiller population was allowed to self-

cross. Seeds were harvested and grown up in staggered batches in short day for mutant identification through thermal imaging and subsequent DNA extraction.

Chapter 1 is co-authored with Dr. Paulo Ceciliato, Felipe Rangel, Morgana Sidhom, and Li Zhang. The thesis author was the primary author of these chapters.

Chapter 2 Completion of Investigation of the Role of SBTs in *Brachypodium distachyon* utilizing Sodium Azide Sequenced Mutant Lines

Development of stomatal pores is regulated by several genes, in particular those belonging to the *EPF* (Epidermal Patterning Factor) gene family which inhibits stomatal development when active. *EPF* family genes, or more specifically *EPF2* has been shown to be activated after being cleaved by members of the *SBT* (Subtilisin-like protease) gene family; however, the specific

function of this gene family in *Brachypodium distachyon* has yet to be elucidated. In an effort to determine which of these genes may play an important role in the upregulation of stomatal development inhibition, a population of NaN (Sodium Azide) mutagenized lines was used. Sequence indexed NaN lines were selected based mutations predicted to have been both impactful and sustained within a member of the SBT gene family to investigate stomatal density in grasses. Of the 11 lines predicted to have sustained a mutation within the SBT gene family, 9 were confirmed to contain the predicted mutation. All lines characterized were shown to be wildtype-like in thermal imaging and stomatal index and density calculations. Intact leaf gas exchange was pursued for 2 of the mutant lines including the only double mutant within the population, and in both cases NaN lines were shown to be wildtype-like. A phenotype could not be observed for any line within the population, possibly due to genetic redundancy present within the SBT family.

2.1 Introduction:

While it has been shown previously that increased atmospheric CO_2 concentrations induces stomatal closing, there are other potential consequences to this phenomenon. It has also been shown that plants grown under high CO_2, or those that have been exposed for long periods of time, tend to develop fewer stomata on leaf surfaces (F. I. Woodward, 1987). Historically, stomatal density and size have been directly related to relative CO2 concentrations. In times of decreased concentrations plants had smaller but more numerous stomata, while during increased concentrations there are fewer stomata present on leaves, but they are considerably larger (Doheny-Adams et al., 2012).

Stomatal density is controlled by the *EPF* (Epidermal Patterning Factor) genes, or more specifically *EPF2*. *EPF2* has been shown to be upregulated by increased CO_2, but is also known to suppress stomatal development, instead promoting formation of pavement cells (Doheny-Adams et al., 2012; Engineer et al., 2014). *EPF2* is activated after cleavage by upstream SBT genes (Subtilisin-like protease) and after activation, initiating a signaling cascade ultimately inhibiting further stomatal development. This has been supported by generation of an *epf2* mutant line, in which more stomata were present than on the wildtype control (Engineer et al., 2016).

The stomatal development pathway has been well researched in *Arabidopsis* including identification of major contributors to stomatal pore and guard cell development, controlling stomatal formation. Genes such as AtSPCH (Speechless), AtMUTE and AtFAMA (retinoblastoma related) are all involved in the development of guard cells and promote differentiation into this pathway (Raissig et al., 2016). Other genes such as *EPF* and *CLV3* (CLAVATA 3) also contribute to this pathway and mediate proper stomatal density and spacing on leaf surfaces through cell-cell signaling. This interaction triggers a downstream signal cascade to be mediated by phytohormones

dependent on plant development (Deng et al., 2020). *SPCH* functions as the initiation step in lineage development of stomatal cells and the subsequent divisions leading to differentiation. This step is followed by *MUTE,* which determines the fate of the GMC (Guard Mother Cells) in tandem with other genes contributing to proper stomatal development (Deng et al., 2020).

Earlier in the signaling cascade, however, is *EPF2*, which when active begins a different cascade working in opposition to *SPCH* and ultimately causes inactivation (Chater et al., 2017). While this pathway is very well known in *Arabidopsis*, the same does not hold true for *Brachypodium*. In fact, even though several orthologues are present in *Brachypodium*, they have been shown to have less functional redundancy among them and tend to be more specialized (Raissig et al. 2016; Chater et al. 2017). Such is the case for the differences between *AtMUTE* (*Arabidopsis*) which allows for the formation of GMC, and *BdMUTE* (*Brachypodium distachyon*) which leads to the generation of subsidiary cells that contribute to stomatal movement in a cooperative manner with guard cells (Raissig et al., 2016, 2017).

Unlike the stomata found within Arabidopsis, grasses contain dumbbell-shaped stomata allowing them to respond to their environment faster and at a lower energetic cost. This is thought to be due to the shape, and also to the presence of the subsidiary cells making up the other portion of the stomatal pore on grass leaves (Raissig et al., 2017). Further characterization of these *Brachypodium* orthologues originally discovered in *Arabidopsis* may lead to improved water use efficiency to be extended to crops promoting sustainable food production (Y. Wang & Chen, 2020).

In an effort to begin work in characterizing the genes that are necessary and sufficient to modulate stomatal development utilizing the grass reference model *Brachypodium distachyon*, characterization of a mutant population was pursued. A library of sequence indexed NaN (Sodium Azide) mutagenized lines was created by JGI Phytozome to be characterized to determine if a

mutant containing more numerous or larger stomata could be identified. NaN was utilized because it has been shown to be very useful in barley and tends to have a very high mutagenic frequency. It has also been observed that it contains little to no chromosomal aberrations, and is creates almost exclusively base substitutions, with little to no frame shift mutations occurring (Olsen et al., 1993).

During the characterization of the NaN lines, only those which had been selected by previous lab members that were predicted to have sustained an impactful mutation within the SBT gene family were selected. It was hypothesized that mutations within this gene family would lead to mutants containing more stomata assuming there is not redundancy by others within the family.

2.2 Results:

2.2.1 Characterization of promising sodium azide sequence indexed mutants

Plants that have spent an extended amount of time exposed to high CO_2 on average have fewer stomata present on the surface of leaves. This processed is controlled by the peptide EPF2 and the enzymes that activate it are called SBTs (subtilisin-like protease) (Engineer et al., 2014). This is well stablished in Arabidopsis, but whether a similar signaling pathway plays a role in grasses is unknown. Lines selected by a previous team member were predicted to have sustained impactful mutations in the SBT gene family. Mutations within that gene family were selected as the SBTs were discovered in *Arabidopsis thaliana* and were found to upregulate downstream protein EPF2 (Epidermal Patterning Factor 2). EPF2 functions to inhibit development of stomata once cleaved and activated by SBTs. Therefore, by utilizing mutants containing an impactful mutation in one of the SBTs, it was hypothesized that plants would contain more stomata. As such, to quantify phenotypes stomatal imaging was performed on NaN mutagenized lines compared to wildtype (Bd 21-3) and statistical analyses (ANOVA) were run after completion of 3 replicates to determine significance. Slides were made from an epidermal peel of the abaxial side of the leaf used for imaging and images were used to calculate stomatal index and density for all the following mutants. Line names, positions, and predicted mutations were obtained through JGI Phytozome.

The first line analyzed was line NaN 1688, which was predicted to have a high impact mutation leading to a premature stop codon was imaged. But it was not shown to contain significant differences in stomatal index or density compared to wildtype after being analyzed using ANOVA (Figure 2.1). NaN2011 was predicted to contain a missense mutation leading to a codon change from cysteine to threonine was also imaged under the same conditions and grown alongside wildtype for comparison. Following ANOVA analyses, neither stomatal index nor

density were shown to be statistically different when compared to wildtype Bd 21-3 (Figure 2.2). Line NaN87 was also predicted to contain a missense mutation leading to an amino acid change, glycine to alanine. Although the p-value obtained through running the ANOVA determined that neither stomatal index nor density were significantly different from Bd 21-3 (Figure 2.3). NaN397 was predicted to contain the same nonsense mutation of a glycine to alanine as observed in NaN87, but present in a downstream gene. However, like the others neither stomatal index nor density were shown to be significantly different based on the p-value obtained through running the ANOVA (Figure 2.4).

To determine if plants were perhaps more efficient at gas exchange though they were not shown to have a higher amount or more densely clustered stomata, intact leaf gas exchange analyses were pursued by another team member. It can be observed in Figure 2.5 that the steady state stomatal conductance values are very similar for both NaN397 and Bd 21-3. All of the NaN lines characterized were single mutants with the exception of NaN310, which was predicted to have sustained point mutations in 2 different genes. The predicted mutations included amino acid changes from cysteine to alanine, and a cysteine to threonine. After completing the ANOVA, NaN310 was also shown not to be significant for either stomatal index or density calculations (Figure 2.6). Being the only double mutant, NaN 310 was predicted to have the strongest phenotype, but since it was not shown to contain more stomata per image, it was hypothesized that it may have more stomata containing rows of cells per leaf. Stomata containing rows was calculated using the same images used above, and data were shown to be almost identical (Figure 2.7).

As EPF2 has been shown to inhibit stomatal development when active, stomatal length was also measured to determine if stomata on the surface of leaves were larger instead of more

numerous. Using the previous images from initial stomatal imaging, length was also measured using a ruler function within Image J. Data were also analyzed utilizing an ANOVA test, which determined that the length was not significantly different when compared to wildtype, counterintuitively stomata appear to be slightly shorter (Figure 2.8). As gas exchange analyses are much more robust than stomatal index and density calculations, stomatal conductance analyses were also pursued. Steady state stomatal conductance measured by NaN310 was not shown to be markedly different from wildtype; but was shown to be slightly lower as observed in Figure 2.9. All lines characterized were compiled into a table showing the gene and gene family affected, predicted mutation, thermal imaging, and stomatal phenotype observed. The table has been adapted from preliminary work completed by previous lab members; updates, including completion of observed developmental phenotypes of stomata have been notated in blue (Table 2).

A

Line	NaN1688_Bd173037681_Hom
Position of mutation	Bd1: 73037680…73037682 (Hom)
Mutation	C > T tgG/tgA
Type of mutation	Nonsense (premature stop)
Predicted effect impact	High

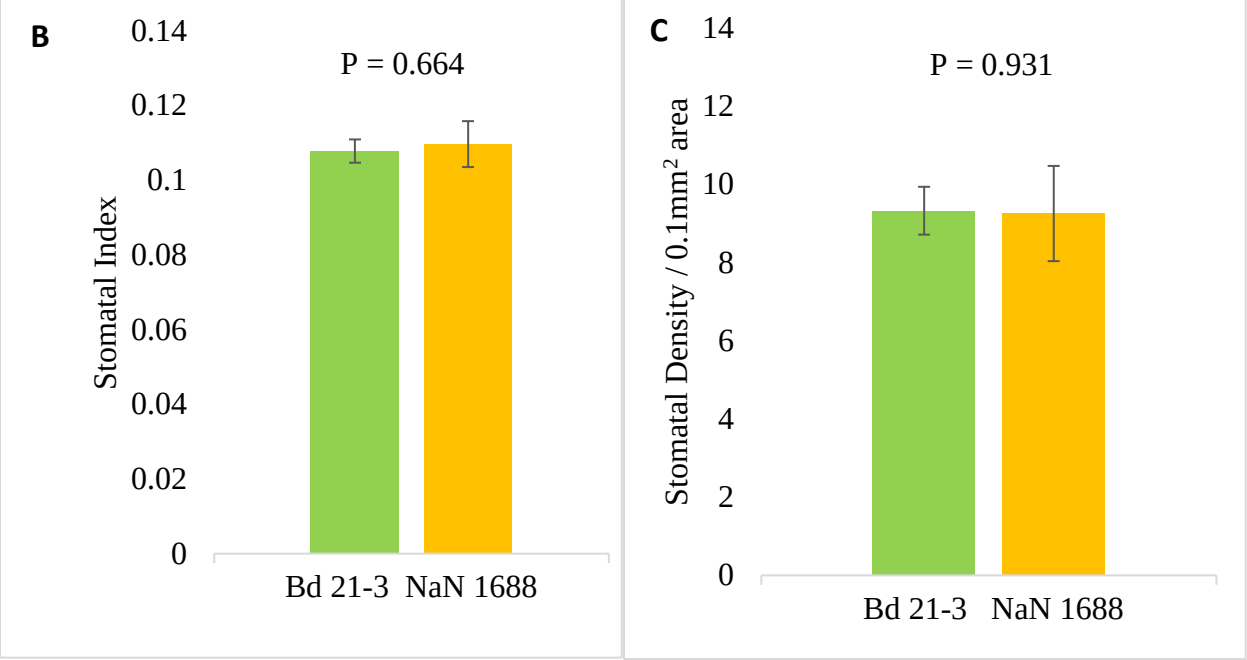

Figure 2.1: Stomatal index/density calculations for sodium azide (NaZ) mutagenized line NaN 1688 (Bradi1g75550; SBT1.3/SDD1) compared to wild-type (Bd 21-3).

Average stomatal index and stomatal density ± standard deviation was calculated using three experimental repeats using a minimum of 5 plants per repeat for NaN 1688 and a minimum of 5 plants per experiment for Bd21-3 (wild-type). Analysis included 4 images per plant. Images were taken of the 4th true leaf from the NaN 1688, and parental Bd21-3 (wildtype) lines 28 dag (days after germination). Leaves were imaged at 40x magnification. Predicted mutation site, type, and effect are listed, A) obtained from Phyotozome. Associated p-values are B) 0.664 and C) 0.931 for stomatal index and density respectively for NaN 1688 compared to wildtype Bd 21-3 (single factor ANOVA).

A

Line	NaN2011_Bd1_11974587_Hom
Position of mutation	Bd1: 11974586…11974588 (Hom)
Mutation	C > T Gac/Aac
Type of mutation	Missense (non-synonymous)
Predicted effect impact	Moderate

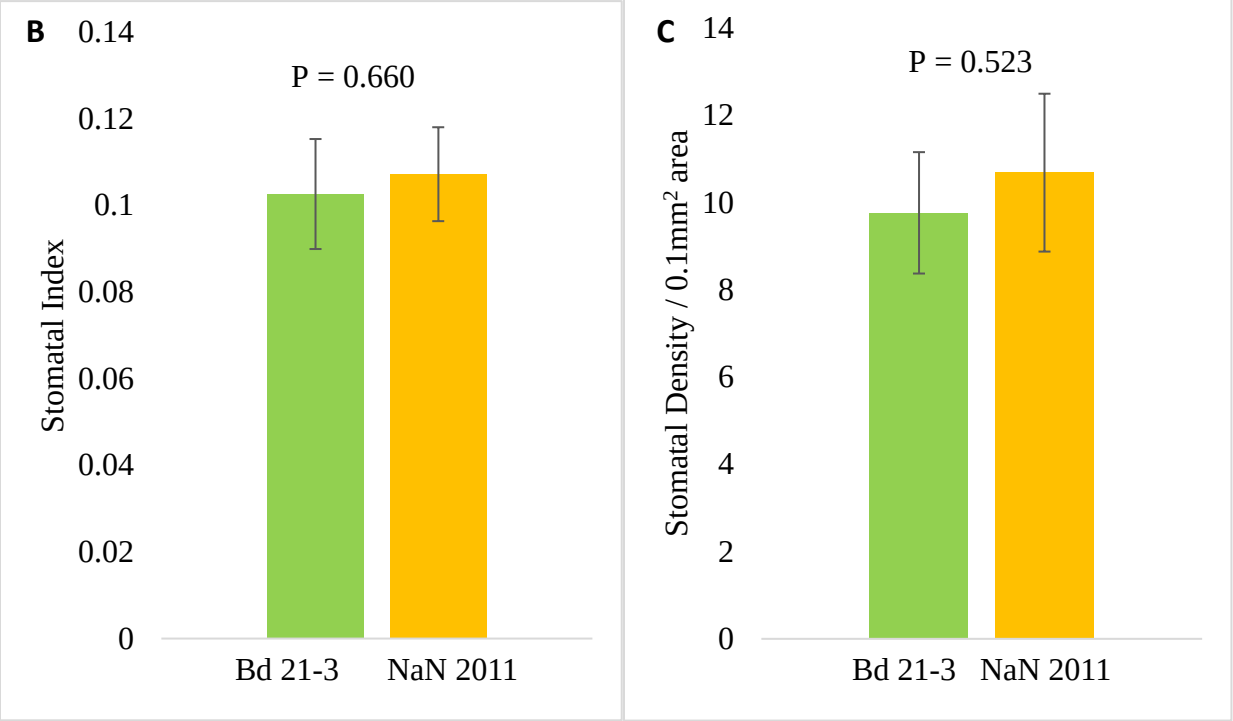

Figure 2.2: Stomatal index/density calculations for sodium azide (NaZ) mutagenized line NaN 2011 (Bradi1g14860, SBT1.7).

Average stomatal index and stomatal density ± standard deviation was calculated using three experimental repeats using a minimum of 3 plants per repeat per line. Images were taken of the 4th true leaf from the NaN 2011, and parental Bd21-3 (wildtype) lines 28 dag (days after germination) at 40x magnification. Analysis included 4 images per plant. Predicted mutation site, type, and effect are listed, A) obtained from Phyotozome. Associated p-values are B) 0.660 and C) 0.523 for stomatal index and density respectively for line 2011 and Bd 21-3 (single factor ANOVA).

A

Line	NaN87_Bd1_11976653_Hom
Position of mutation	Bd1: 11976652…11976654 (Hom)
Mutation	G >A gCg/gTg
Type of mutation	Missense (non-synonymous)
Predicted effect impact	Moderate

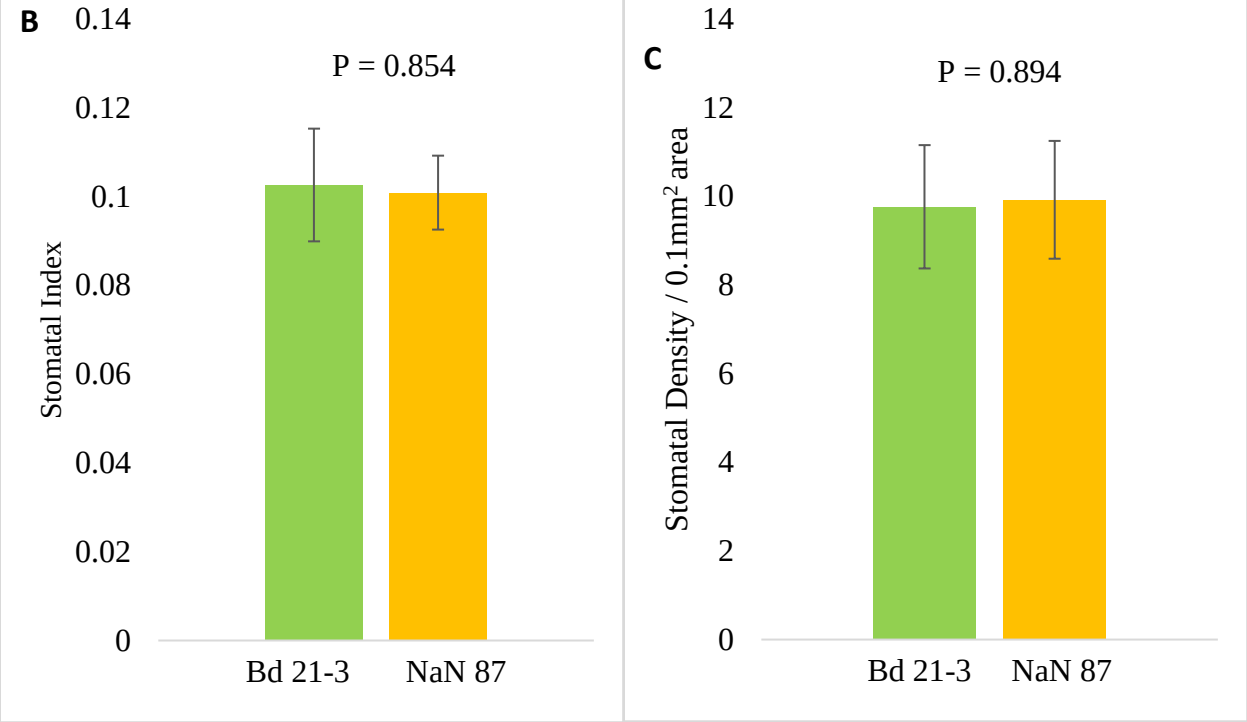

Figure 2.3: Stomatal index/density calculations for sodium azide (NaZ) mutagenized line NaN 87 (Bradi1g14860, SBT1.7) compared to wild-type (Bd 21-3).

Average stomatal index and stomatal density ± standard deviation was calculated using three experimental repeats using a minimum of 3 plants per repeat per line. Images were taken of the 4th true leaf from the NaN 87, and parental Bd21-3 (wildtype) lines 28 dag (days after germination) at 40x magnification. Analysis included 4 images per leaf for NaN line 87 and Bd 21-3 (wildtype). Predicted mutation site, type, and effect are listed, A) obtained from Phyotozome. Associated p-values are A) 0.854 and B) 0.894 for stomatal index and density respectively for NaN line 87 when compared to wildtype Bd 21-3 (single factor ANOVA).

A

Line	NaN397_Bd4_30100875_Hom
Position of mutation	Bd4: 30100874…30100876 (Hom)
Mutation	G >A gGc/gAc
Type of mutation	Missense (non-synonymous)
Predicted effect impact	Moderate

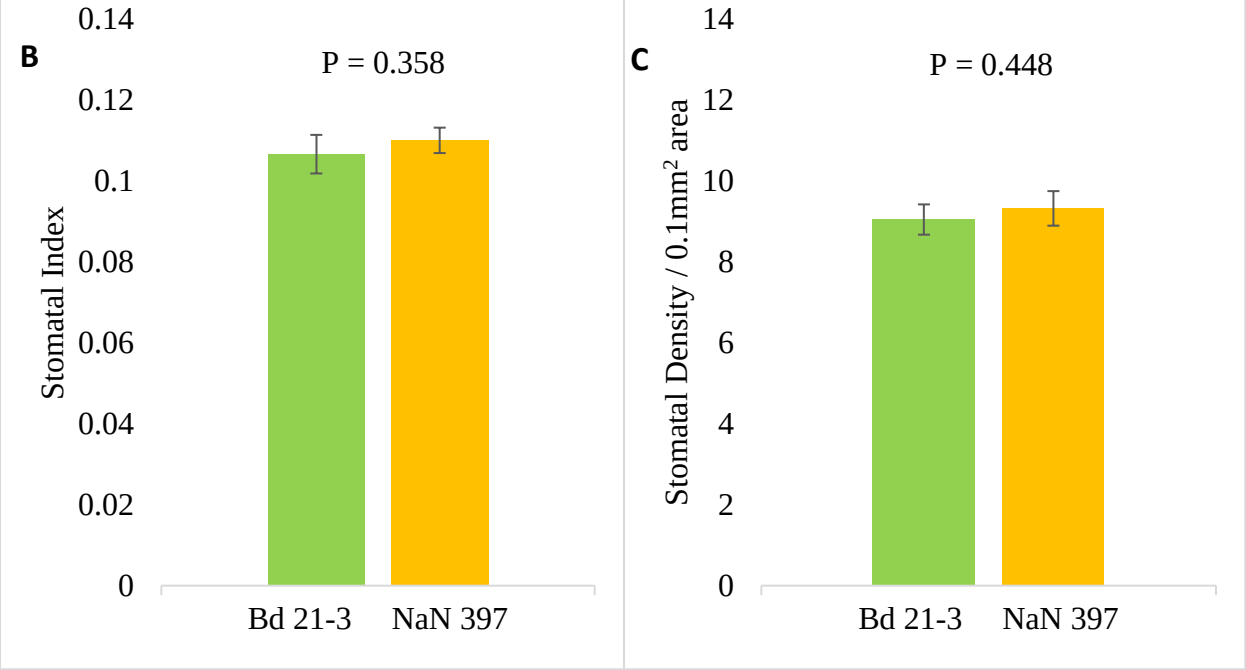

Figure 2.4: Stomatal index/density calculations for sodium azide line NaN 397 (Bradig4g24790, SBT1.7) compared to wild-type (Bd21-3).

Average stomatal index and stomatal density ± standard deviation was calculated using three experimental repeats using a minimum of 5 plants per line for NaN 397 and Bd21-3 (wildtype). Images were taken of the 4th true leaf from the NaN 397 and parental Bd21-3 (wildtype) lines 28 dag (days after germination). Leaves were imaged at 40x magnification. Analysis included 4 images per plant for each line. Predicted mutation site, type, and effect are listed, A) obtained from Phyotozome. Associated p values are A) 0.358 and B) 0.448 for stomatal index and density respectively for line NaN 397 compared to Bd 21-3 (single factor ANOVA).

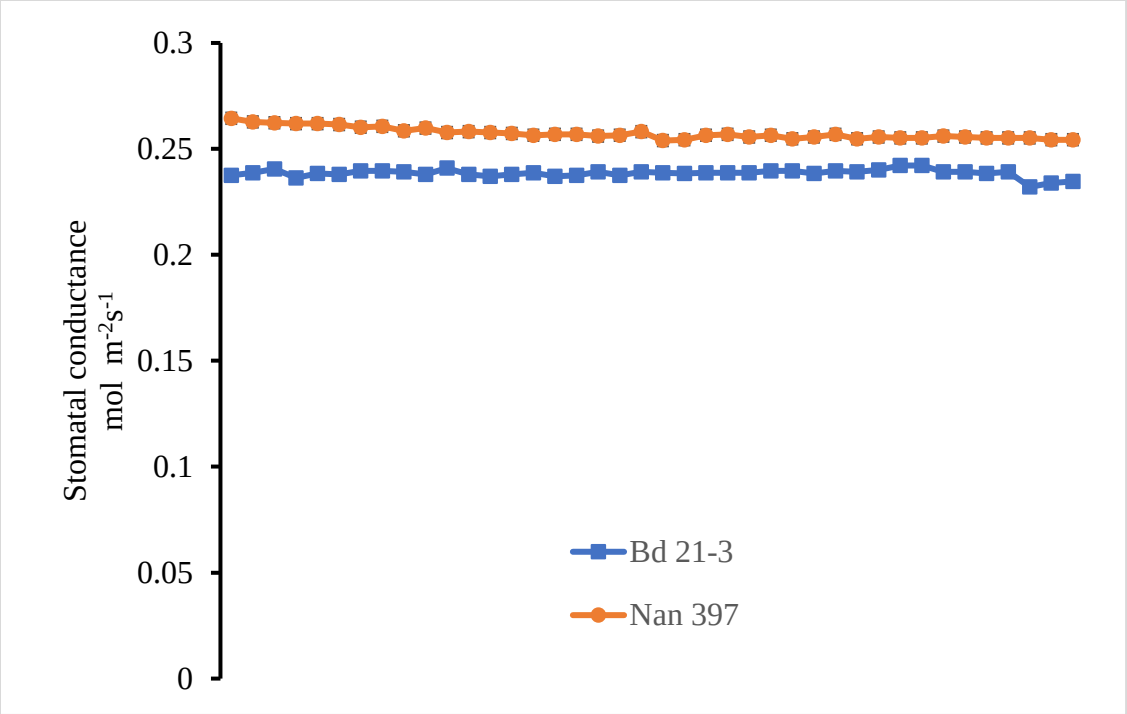

Figure 2.5: Time-resolved stomatal conductance analysis of the NaN 397 line (Bradig4g24790, SBT1.7) (with Dr. Paulo H. O. Ceciliato)

Time-resolved stomatal conductance analyses after 60 minutes of insertion of leaves into a gas exchange analyzer chamber. Wild-type (Bd21-3), NaN 397 line were analyzed using whole-leaf gas exchange analyses. Stomatal conductance in mol m^{-2} s^{-1}. Data shown were normalized to the average of the first 5 minutes of stomatal conductance values recorded. N=4 leaves ± SD through N=3 repeats.

A

Line**	NaN310_Bd4_39154932
Position of mutation	Bd4: 39154931…39154933 (Hom)
Mutation	C >A tCc/tAc
Type of mutation	Missense (non-synonymous)
Predicted effect impact	Moderate
Line**	NaN310_Bd1_11974572_Hom
Position of mutation	Bd1: 11974571…11974573 (Hom)
Mutation	C >T Gag/Aag
Type of mutation	Missense (non-synonymous)
Predicted effect impact	Moderate

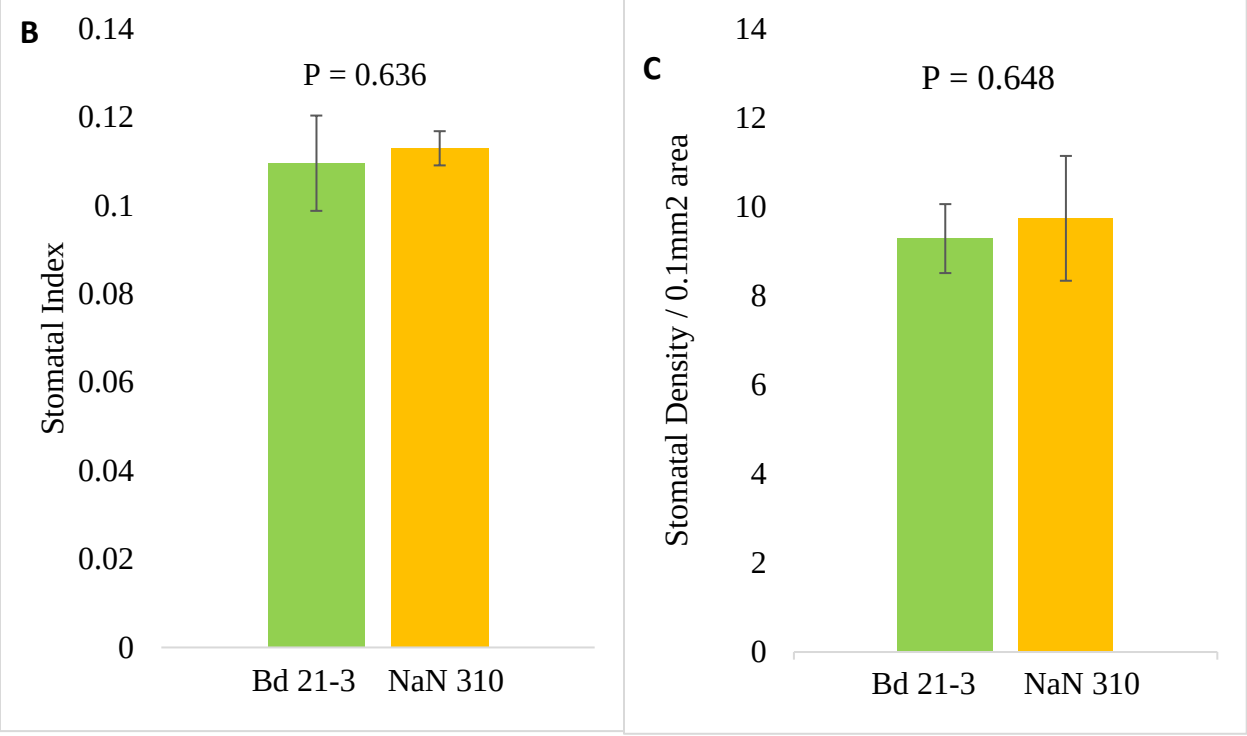

Figure 2.6: Stomatal index/density calculations for sodium azide (NaZ) mutagenized line NaN 310 Bradi4g33237 (SBT 5.3) and Bradi1g14860 (SBT 1.7) compared to wild-type (Bd 21-3).

Average stomatal index and stomatal density ± standard deviation was calculated using three experimental repeats using a minimum of 3 plants per repeat per line. Images were taken of the 4th true leaf from the NaN 310, and parental Bd21-3 (wild-type) lines 28 dag (days after germination) at 40x magnification. Predicted mutation site, type, and effect are listed, A) obtained from Phyotozome. ** Indicates both mutations sustained by NaN 310 double mutant line affected in 2 different SBT genes (1.7 and 5.3). Analysis included 4 images per leaf. Associated p-value is B) 0.636 and C) 0.648 for stomatal index and density, respectively, for NaN 310 when compared to Bd21-3 (single factor ANOVA test).

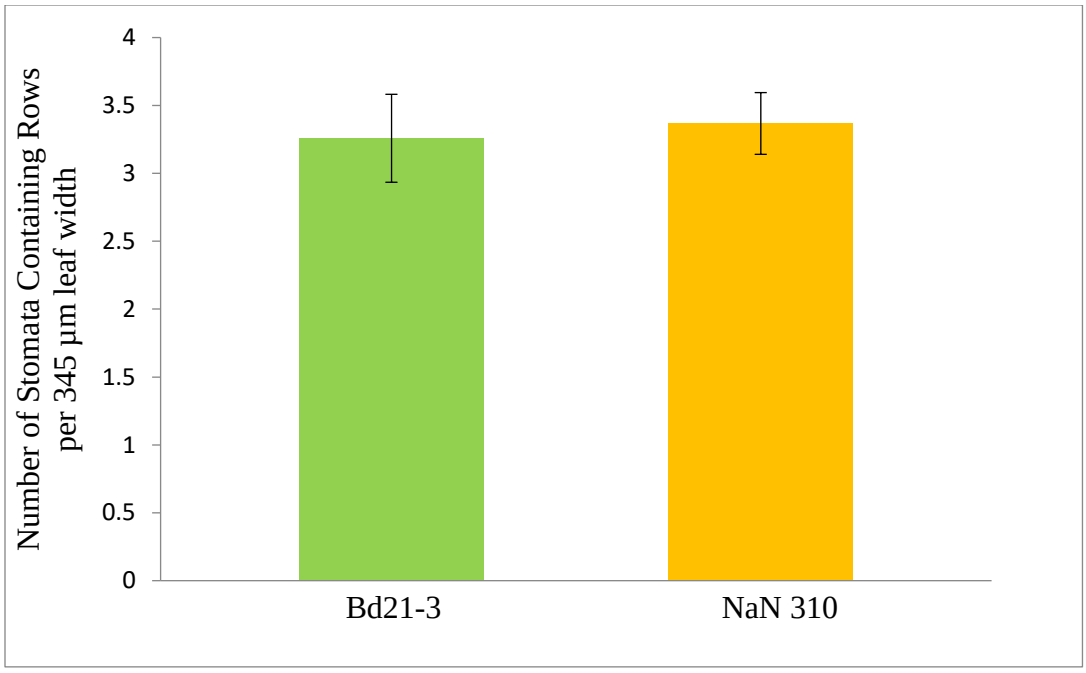

Figure 2.7: Number of stomata containing rows per 345 µm leaf width for sodium-azide mutagenized line NaN 310 Bradi4g33237 (SBT 5.3) and Bradi1g14860 (SBT 1.7) is comparable to wild-type (Bd21-3).

Stomatal spacing and morphology for NaN 310 is wild-type-like. The average of the number of rows containing stomata per line was calculated using two experimental repeats of a minimum of n≥5 plants per line, 4 images each plant, of the 4th true leaf from the NaN 310 and parental wild-type (Bd21-3) lines 28 dag (days after germination). Leaves were imaged at 40x magnification.

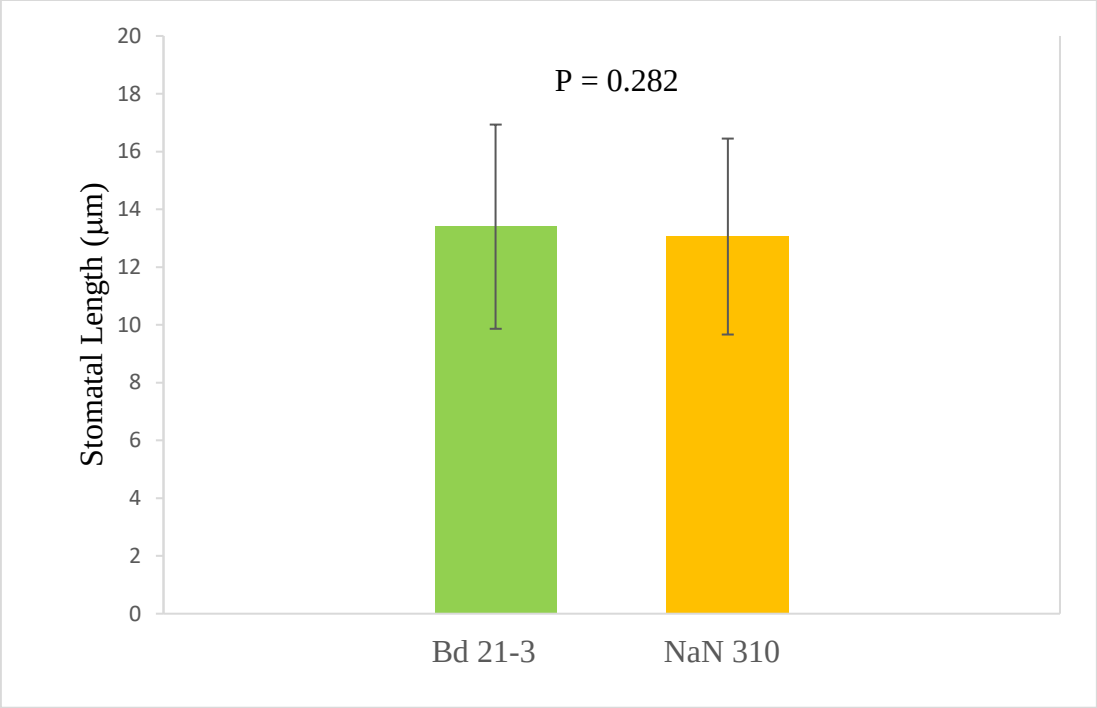

Figure 2.8: Stomatal length for sodium-azide mutagenized line NaN 310 Bradi4g33237 (SBT 5.3) and Bradi1g14860 (SBT 1.7) is comparable to wild-type (Bd21-3).

Stomatal height is shown to be comparable to wildtype. The average of the height of stomata per leaf was calculated using three experimental repeats of a minimum of n≥3 plants per line utilizing the 4th true leaf from lines NaN 310 and parental wild-type (Bd21-3) lines 28 dag (days after germination). Analysis included 4 images per leaf at 40x magnification. Height was standardized utilizing a ruler and measured within Image J. Associated p-value is 0.282 when compared to wildtype (single factor ANOVA).

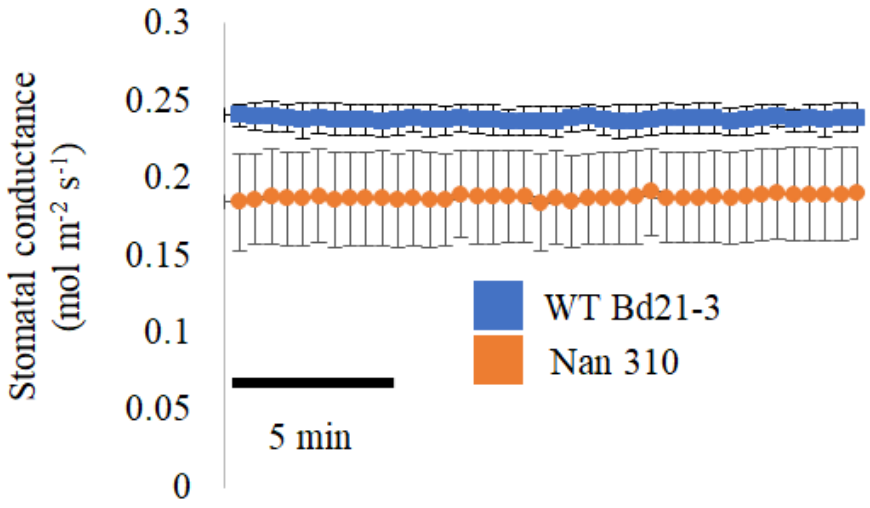

Figure 2.9: Time-resolved stomatal conductance analysis of the NaN 310 line (Dr. Paulo H. O. Ceciliato).

Time-resolved stomatal conductance analyses after 60 minutes of insertion of leaves into a gas exchange analyzer chamber. Wild-type (Bd21-3) and Nan 310 line were analyzed using whole-leaf gas exchange analyses.
Stomatal conductance in mol m^{-2} s^{-1}. Data shown in were normalized to the average of the first 5 minutes of stomatal conductance values recorded. N=3 leaves ± SD.

Table 2: NaZ lines predicted to be most promising selected for genotyping and phenotyping Preliminary work completed by Morgana Sidhom.

Lines represented in this table are those predicted to have sustained impactful mutations that were also used in experiments. Predictions were based on sequencing data obtained from JGI Phytozome's database, updated November 2018. Data presented in blue represent updates to preliminary work completed by Morgana Sidhom.

*** Notates that a given column may contain additional comments specific to a given line such as issues that may impact future experimentation.

NaN Lines Loci	Gene of Interest	Gene Family	Amino Acid/Codon Change	Thermal Imaging	DIC stomatal imaging (preliminary, N=1, N=2, N=3***)	Stomatal Development Phenotype ***
NaN1688 Bd1:73037680..73037682 (Hom)	Bradi1g75550	SDD1/SBT 1.3	Unconfirmed (more seeds are being bulked)	wild type-like	N=3	wild-type-like
NaN2011 **Position** Bd1:11974586..11974588 (Hom)	Bradi1g14860	SBT 1.7	Gtc/Atc V102I ongoing	wild type-like	N=3	wild-type-like
NaN87 Bd1:11976652..11976654 (Hom)	Bradi1g14860	SBT 1.7	unconfirmed	wild type-like	N=3	Wild-type-like
NaN310 Bd1:11974571..11974573 (Hom)	Bradi1g14860	SBT 1.7	aAG/aGA R19E Gag/Aag E723K	wild type-like	N=3	wildtype-like

Table 2: NaZ lines predicted to be most promising selected for genotyping and phenotyping Preliminary work completed by Morgana Sidhom, Continued.

NaN Lines Loci	Gene of Interest	Gene Family	Amino Acid/Codon Change	Thermal Imaging	DIC stomatal imaging (preliminary, N=1, N=2, N=3***)	Stomatal Development Phenotype ***
NaN310 Bd4:39154931..39154933 (Hom)	Bradi4g33237	SBT 5.3	tCc/tAc S247Y			
NaN397 Bd4:30100874..30100876 (Hom)	Bradi4g24790	SBT 1.7	gGc/gAc G307S	wild type-like	N=3	wild-type-like
NaN1949 Bd1:5573606..5573608 (Hom)	Bradi1g07700	SBT 5.2	Gcc/Acc A359T	wild type-like	N=1, low germination	Out of seeds, very low germination rate, would not grow.
NaN448 Bd4:45694124..45694126 (Hom)	Bradi4g41420	SBT 1.8	gCg/gTg A567V	wild type-like	N=1, low germination	Very low germination, those that grew did not set seeds.
NaN418 Bd4:39154234..39154236 (Hom)	Bradi4g33237	SBT 5.3	Gtg/Ttg V112L	wild type-like	N=1, low germination	Very low germination, those that grew did not set seeds.

2.3 Discussion:

Characterization of sequence indexed NaN (Sodium Azide) mutagenized lines which were predicted to have sustained impactful mutations within the SBT (subtilisin-like protease) gene family was initiated by a previous lab member. Utilizing JGI Phytozome's index, lines were identified and predicted mutations could be obtained along with the predicted mutation's impact on gene functionality (https://phytozome.jgi.doe.gov/pz/portal.html). Although the role of the SBTs in *Brachypodium distachyon* has not yet been elucidated, mutants identified in *Arabidopsis thaliana* of the same gene family were shown to have increased stomatal density (Vráblová et al., 2017).

In *Arabidopsis* it can be observed that upstream SBT genes cleave, and thereby activate, *EPF2* causing a downregulation in stomatal development in the presence of CO_2 (Engineer et al., 2014). Different members of the EPF family of proteins have been shown to have differing effects on regulating stomatal development, including positive or negative regulation (Bergmann 2004; Rowe and Bergmann 2010; Peterson, Rychel, and Torii 2010). Therefore, NaN lines were used to determine if the same trend of increased stomatal density could be observed in *Brachypodium* in lines that had sustained mutations in the SBT family.

Many of the lines included in this characterization were genotyped by the preceding lab member. Lines were also analyzed using thermal imaging; results of genotyping and thermal imaging analyses are included in Table 2. Also contained within the table are predicted mutation sites, amino acid change sustained, and gene of interest, and the subfamily the gene belongs to.

Following initial characterization for the NaN lines, stomatal index and density calculations were pursued following stomatal imaging under the DIC microscope. For all 8 lines

analyzed, a phenotype could not be observed for either stomatal density nor index calculations when compared to wildtype (Bd 21-3) (Figures 2.1-2.4 and 2.6). For both lines NaN 310 and NaN 397, intact leaf gas exchange analyses were also pursued, but a phenotype could not be discerned when compared to wildtype (Bd 21-3). Stomatal length and stomata containing rows were also calculated for NaN 310, which was the only double mutant within the sample group, sustaining point mutations in both SBT 1.7 and SBT 5.3 (Table 2). It was hypothesized that NaN 310 being a double mutant would yield a more robust phenotype. It was also speculated that perhaps the phenotype would present in a slightly different manner from what was observed in *Arabidopsis*, which is why follow up tests were pursued. However, none of the experiments run on any NaN line tested within the SBT gene family were shown to present a phenotype markedly different from wildtype, at least not one which was reproducible.

Even grown under conditions thought to be ideal, some lines showed very poor germination, such as lines NaN 418, 448, and 1949, for which stomatal imaging analyses could not be completed. NaN 1949 showed very low germination rates even under well-watered conditions, and sowing only after being cold treated at 4°C for a minimum of 7 days. Lines NaN 418 and NaN 448 also had low germination rates, and even under the same conditions as other plants, appeared to be weaker and did not often set seeds. Due to the low germination rates and difficulty replacing seed stocks, analyses were discontinued when seed stocks were depleted.

As none of the mutants characterized showed reliable or reproducible phenotypes, it was concluded that the mutations sustained may not be as impactful as originally thought by lab members, or predicted by JGI Phytozome (https://phytozome.jgi.doe.gov/pz/portal.html).

However, it is possible that a phenotype could be seen in the event that several genes were knocked out. Gene redundancy could play a role if genes possess overlapping functionality or have

highly correlated expression (García-Marqués et al., 2016). If the affected genes have shared functionality with at least 1 co-expressed gene, it could be that genetic redundancy between the genes has inhibited a phenotype from being observed through compensation of the functional gene product. A robust phenotype may be able to be obtained if generation of a higher order mutant was obtained through crossing. Due to the difficulty of crossing *Brachypodium* and the lack of an observable phenotype, crossing was not pursued for this population and experimentation concluded.

Use of an amiRNA line may be useful for further experimentation in determining if the SBT genes play a crucial role in determination of stomatal development in *Brachypodium distachyon*. Use of amiRNA lines would allow for several sequentially similar lines to be targeted and knocked down at once, circumventing the issue of gene redundancy. Redundancy was predicted to play a large role in why the NaN lines did not appear to show a phenotype for any line, not even those which had been genotyped and confirmed to contain the mutation. If a phenotype could be observed with an amiRNA targeting several of the SBTs, it may be worth generating stable mutant lines, although a phenotype could not be ascertained in this screen.

2.4 Methods:

1. DIC Imaging and Stomatal analyses

2.4.1 DIC Imaging and Stomatal analyses

Stomatal imaging was conducted by following an epidermal peel technique developed by Morgana Sidhom and Felipe Rangel. The 4th true leaf from healthy 5-6 week old *Brachypodium distachyon* plants was selected for imaging. Imaging was done utilizing slides of the imprint of the abaxial side of leaves. Slides were created using super glue (Loctite Super Glue) and pressing the leaf evenly onto slides and peeling off the leaf once dry. Resulting imprint was then imaged using the DIC (Differential Interference Contrast) microscope and attached camera. A minimum of 4 images were taken per leaf imprint at 40x magnification. At least 3 plants were used per genotype per experiment. The "cell-counter" function within Image J was used to count stomata and pavement cells within images. Data collected from stomatal imaging allowed for index, density, and stomatal containing rows. A pixel counting measurement tool within Image J was used to measure stomatal length of images generated from the DIC microscope.

Chapter 2 is co-authored with Morgana Sidhom.The thesis author was the primary author of these chapters.

Chapter 3 Identification of F-Box Genes Implicated in ABA Response

Another stress-inducing stimulus that rapidly induces stomatal closure is a phytohormone known as ABA (abscisic acid), which is observed in the presence of drought stress. ABA has been shown to lead not only to stomatal closure, but also inhibits germ ination and promotes seed

dormancy. Although the ABA signaling pathway has been extensively studied, not all components have been identified. Therefore, to find key elements involved in unknown parts of the pathway, an amiRNA (artificial microRNA) screen was conducted to find mutants that germinated in the presence of ABA, indicating reduced sensitivity. Through the screen a very promising mutant was identified, and the amiRNA construct contained within it was shown to target 5 genes of unknown functionality from the F-Box gene family. Stable mutant lines have been created in an effort to identify which genes of the 5 are responsible for the phenotype, and to ascertain how their role *in vivo* may contribute to the ABA pathway. Preliminary data shows the most promising lines may be implicated in regulation of key components leading to perception and response to drought. A triple mutant was obtained through transforming a *f-box 1/4* double mutant with a CRISPR construct targeting *F-Box 3*. 3 CRISPR positive lines were identified, from which seeds were collected and utilized in a germination assay alongside wildtype and the original amiRNA mutant line. Germination assay results appear to show recovery of the phenotype observed in the amiRNA screen, indicating that F-box genes 1,3, and 4 are necessary in the ABA signaling pathway. Identification of the specific function of these 3 genes may elucidate unknown mechanisms of regulation of the ABA pathway, allowing for generation of plants that display increased water use efficiency (WUE). This increased WUE can potentially combat increasing water scarcity in agriculture, perhaps circumventing yield penalties observed in drought stressed crops.

3.1 Introduction:

Increasing water scarcity has become a problem of growing magnitude worldwide, especially in the face of the increasing human population, creating a larger need for readily available clean water (Mekonnen & Hoekstra, 2016). Plants must be able to adapt to an ever-changing environment through strict regulation of internal signaling pathways to maintain homeostasis. Plants are able to respond to drought by increasing relative water use efficiency inversely to water availability (Yang et al., 2016). When plants perceive drought in the roots, the phytohormone ABA (abscisic acid) is produced and perceived in leaf tissues, leading to closure of stomata to prevent further water loss (Davies & Zhang, 1991). This perception of ABA in shoots causes differential expression of genes as a focused stress response, especially in the guard cells which are responsible for regulating stomatal opening and closing (Christmann et al. 2005; 2007).

Stomata are pores that function as valves facilitating gas exchange that allows for intake of CO_2 and efflux of water and O_2 back into the atmosphere (Daszkowska-Golec & Szarejko, 2013). Each stomate has 2 surrounding guard cells that will shrink under stressful conditions, facilitating stomatal closure. Stomatal closure caused by shrinking of guard cells is obtained by opening of anion channels after perception of ABA leading to depolarization of the membrane, activating cation channels and the sudden efflux of K+ ions. Cation efflux leads to shrinking of the cells as water follows the solute across the membrane and out of the guard cells, lessening turgor pressure (Daszkowska-Golec & Szarejko, 2013; Malcheska et al., 2017). Stomatal closing is one of the earliest responses to dehydration stress and prevents excess water loss and desiccation through stomatal pores (Daszkowska-Golec & Szarejko, 2013).

ABA has many uses within plants including germination delay, response to drought and salinity, stomatal and gene regulation, and the ability to maintain turgor pressure (Kang et al., 2010; Kuromori et al., 2010; Sharp, 2002). In the presence of ABA, seeds have been shown to maintain dormancy to prevent germination in an environment unsuitable for growth (Seo et al., 2009). This can be exploited during experimentation to find mutants that are less sensitive to ABA, as mutant lines show higher germination rates than wildtype when exposed to exogenous ABA (Rock and Zeevaart 1991; Seo et al. 2006).

Perception of ABA begins with the receptors, PYR/PYL/RCAR (Pyrabactin resistance/Regulatory Component of ABA Receptor) which become active after binding to endogenous ABA (Hauser et al., 2017; Ma et al., 2009). Once active will bind and inhibit downstream negative regulators of the ABA pathway known as PP2Cs (Clade A type 2 protein phosphatases) (Ma et al., 2009; Park et al., 2009). Inhibition of the PP2Cs leads to phosphorylation and activation of OST1/SnRK2 (Open Stomata 1) which serve to phosphorylate and activate downstream stress resistance genes (Hauser et al., 2017). However, OST1/SnRK2 cannot auto-phosphorylate, and therefore activation of *SLAC1* requires outside phosphorylation of OST1/SnRK2, obtained via M3Ks (Map Kinase Kinase Kinase). Reconstitution of this pathway could not be observed in oocytes without the presence of M3Ks, indicating M3Ks are required for propagation of ABA response signals leading to decreased turgor pressure (Takahashi et al., 2020). Takahashi et al (2020) utilized an amiRNA screen as proof of concept to target several homologous genes based on a previous amiRNA screen by Hauser and Ceciliato et al (2019) which was used to identify ABA insensitive mutants (Hauser et al. 2019; Takahashi et al. 2020).

PYR/PYL triple and quadruple mutants have been shown to have increasing ABA insensitivity (Park et al., 2009). It has also been observed that mutations sustained within multiple

PP2Cs lead to hypersensitivity. When ABA is not perceived, PYLs are phosphorylated and tagged for degredation (Yu et al., 2019). A possible proposed mechanism for the degredation of the PYR/PYLs is through a group of F-Box proteins. In *Arabidopsis thaliana,* there are approximately 700 F-Box proteins within the F-Box gene family. These F-box proteins are able to form specific structures that are able to recognize and specifically regulate relative abundances of other proteins contributing to larger biological processes (Hellmann & Estelle, 2002). Functionality for less than 15% of the genes in the F-Box family have been determined; however, in other stress response pathways they have been shown to interact with the ubiquitin 26S proteasome pathway (Gonzalez et al., 2017). F-Box proteins participate in regulation of other pathways by modulation of upstream substrates via targeted degredation. Examples of this degredation can be seen in both the ethylene and jasmonic acid pathways through recruitment, ubiquitination, and subsequent degredation of targeted substrates via the proteasome (Yan et al., 2013). The F-Box gene family participates in many different pathways through varying mechanisms but many of the specific functions remain unknown.

A screen of an amiRNA (artificial microRNA) library of over 11000 T2 ami-RNA lines was previously completed by previous lab members in an effort to identify mutants insensitive to ABA. The screen was composed of amiRNA transformed lines targeting gene families to tackle genetic redundancy (Hauser et al., 2013, 2019).

During the screen, a mutant was identified as amiRNA 347 (AX-347) that was shown to germinate much better than wildtype in the presence of exogenous 0.5μM ABA present on plates. The amiRNA from that line was sequenced and was shown to have targeted 5 genes within the F-Box family, which are here referred to as F-box1 to F-box5. The function of those 5 genes has yet

to be discovered. As the amiRNA construct targeted 5 genes, determination of which genes are necessary and sufficient to replicate the phenotype has been pursued.

After generation of a double mutant line targeting both *f-box1/f-box 4*, the phenotype could be observed but was determined to be weaker following a germination assay. The double mutant was transformed using a vector obtained from Dr. Yunde Zhao containing a CRISPR construct targeting *F-Box 3*. Seeds selected after transformation were genotyped, and CRISPR+ lines were taken into the next generation (T2) where another germination assay was completed to determine if the amiRNA phenotype had been recovered. Preliminary data from the germination assay suggests recovery of the AX-347 phenotype, but genotyping is currently underway to identify homozygous lines.

3.2 Results:

3.2.1 Identification of F-Box genes involved in ABA response

Plants exposed to drought stress will produce ABA (abscisic acid), a phytohormone that allows the plant to perceive and respond to drought. ABA also promotes seed dormancy and when exogenous ABA is applied to seeds it can inhibit or delay germination. In the case of a plant that is ABA insensitive, germination should not be impeded if grown on ABA containing media. Ami-RNA allows for analysis of knock-down lines of closely related genes by using a short microRNA (21 bp) targeting mRNA containing complimentary sequences. This allows for creating knock down lines of a family of related genes to observe the phenotype with lessened compensation caused by redundancy. During a screen of an amiRNA library, line amiRNA-347 was discovered as it showed higher germination than control HsMYO on ABA containing plates (Figure 3.1A). HsMYO is utilized as the control as the amiRNA construct contains no target in *Arabidopsis thaliana.* Quantification of germination over the course of the assay shows that germination is much higher in amiRNA-347 when compared to the control line grown under the same conditions (Figure 3.1B).

After sequencing line 347, the amiRNA was shown to target 5 of the approximately 700 F-box genes present in *Arabidopsis thaliana*. To determine which F-box genes were necessary and sufficient for this phenotype, generation of higher order mutants was needed. A double mutant was created for *f-box 1* and *f-box 4* was generated, but the original phenotype was not replicated from this double mutant line. The double mutant was transformed utilizing a CRISPR-Cas9 construct targeting *F-Box 3* using a vector obtained from Dr. Yunde Zhao. Following transformation, mCherry positive lines were selected under the fluorescent microscope and were grown for PCR based genotyping (Figure 3.2). The strategy for genotyping using PCR and gel electrophoresis was

based on the premise that only genes which had been cut would contain a band on the gel. If the gene was not cut as shown in Figure 3.3, the conditions of the PCR would not allow for complete amplification of the region flanked by the primers. An intact *F-Box 3* gene would be too long for Taq polymerase to complete construction of the complimentary strand during extension. Following PCR, products were run on an agarose gel alongside a 1KB+ ladder and control primers which were used to verify negative results (Figure 3.4). Samples amplified with *F-Box 3* flanking primers for which a band at approximately 450 BP could be observed were selected as positive results and seeds were collected for further selection in the following generation.

Seeds from lines that were identified to have sustained the deletion of *f-box 3* in T1 were collected and reselected under the fluorescent microscope to identify non-glowing seeds. Seeds that no longer glow were predicted to have sustained the truncated gene; but as mCherry is contained within the CRISPR vector, those which have removed CAS9 should no longer glow. Non-glowing seeds were surface sterilized and plated for genotyping to confirm the deletion has been implemented into the germline, and to test for homozygosity in isolated lines. Seeds not selected for genotyping were used in a preliminary germination assay for observation of the phenotype and for comparison to amiRNA line AX347. Preliminary germination data indicate that line 240 germinated well in the presence of ABA 0.75 μm and appears to show recovery of AX347-like phenotype (Figure 3.5).

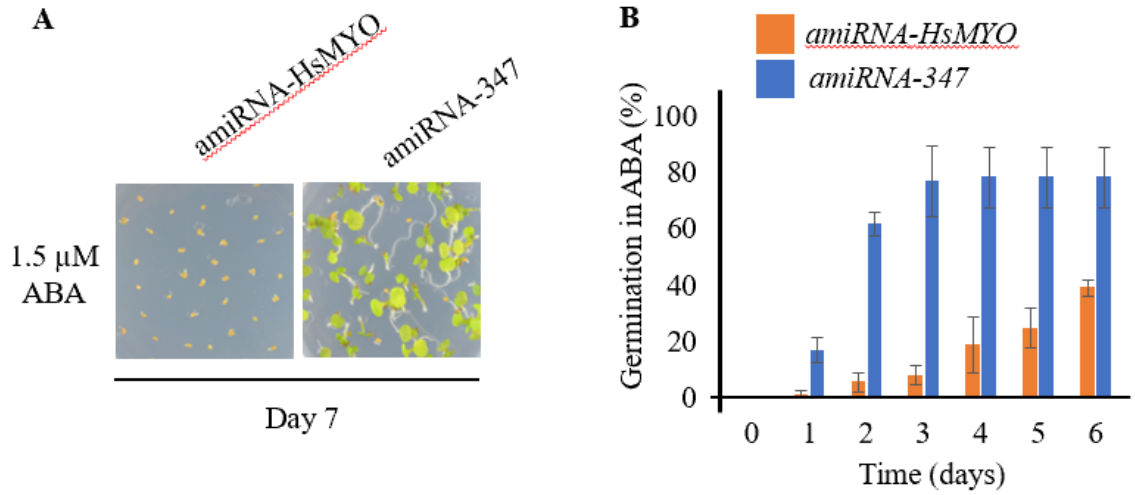

Figure 3.1: The ami-RNA line-347 targeting 5 F-Box genes was shown to be less sensitive to ABA in germination assay. Screen conducted by Dr. Paulo H. O. Ceciliato and Dr. Felix Hauser.

(A) Control line (amiRNA-HsMYO) has no target genes in Arabidopsis (left), and amiRNA-347 targeting 5 F-Box genes which germinated even in the presence of ABA (right) after 7 days of exposure. (B) Quantification of germination assay data obtained from A, presented as percentage of germination.

Figure 3.2: Sequence of genotyping mCherry+ lines.

Previously transformed lines that were shown to be inhibited in f-box1/4 genes were transformed using a CRISPR construct targeting F-box 3. Seeds harvested from transformed plants were selected under the fluorescence microscope to select for those that were mCherry+. Seeds were sterilized and plated onto 1/2MS media. Following cotyledon emergence, seedlings predicted to survive transplantation were transferred to soil. After establishment in soil seedlings underwent DNA extraction and PCR utilizing CRISPR primers flanking the F-box 3 gene and control primers (FER 4 or CPK3) in genes not predicted to be affected by the mutation. Expected band size obtained with CRISPR primers was approximately 450 bp, whereas Fer4 bands were expected to be approximately 1200 bp. Confirmation of positive lines was achieved through a second extraction. Seeds harvested from positive lines will be re-selected under the microscope to identify those which no longer fluoresce.

f-box 1/f-box 4 double mutant lines

Transformed using CRISPR construct to delete F-box 3

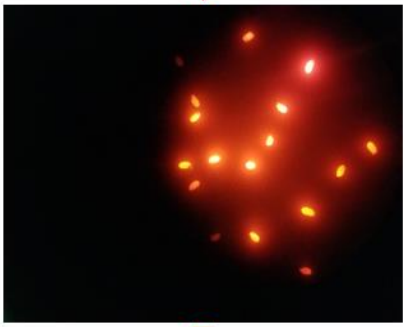

Approximately 300 mCherry+ seeds were selected under the fluorescence microscope

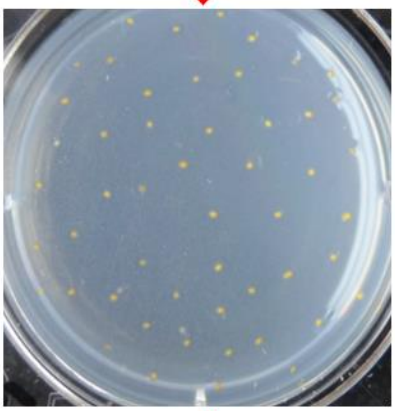

T1 seeds were sterilized and plated onto ½ MS containing media. Approximately 265 seedlings were transferred to soil.

~250 plants underwent DNA extraction and PCR amplification utilizing primers flanking the F-Box 3 gene.

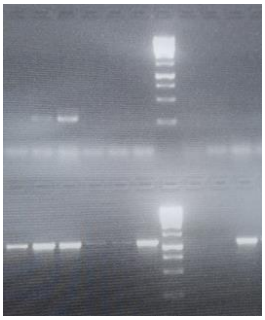

CRISPR primers

Fer4 primers (control)

PCR products were visualized on a 2% gel to identify lines sustaining the cut gene. Those showing positive results were confirmed through a second extraction and PCR.

Seeds harvested from those shown to contain the cut will be reselected under the fluorescence microscope. Selection will be for seeds no longer shown to fluoresce.

Figure 3.2: Sequence of genotyping mCherry+ lines, Continued.

Previously transformed lines that were shown to be inhibited in f-box1/4 genes were transformed using a CRISPR construct targeting F-box 3. Seeds harvested from transformed plants were selected under the fluorescence microscope to select for those that were mCherry+. Seeds were sterilized and plated onto 1/2MS media. Following cotyledon emergence, seedlings predicted to survive transplantation were transferred to soil. After establishment in soil seedlings underwent DNA extraction and PCR utilizing CRISPR primers flanking the F-box 3 gene and control primers (FER 4 or CPK3) in genes not predicted to be affected by the mutation. Expected band size obtained with CRISPR primers was approximately 450 bp, whereas Fer4 bands were expected to be approximately 1200 bp. Confirmation of positive lines was achieved through a second extraction. Seeds harvested from positive lines will be re-selected under the microscope to identify those which no longer fluoresce.

Figure 3.3: Strategy for PCR genotyping of the CRISPR+ lines.

f-box1/f-box 4 double mutant lines were transformed by Dr. Paulo Ceciliato using a CRISPR construct targeting F-Box 3 utilizing a vector obtained from Dr. Yunde Zhao. The vector contained mCherry and 2 guide RNA cassettes facilitating large scale deletions. Transformation efficiency was increased due to a embryo specific promoter for Cas9 also contained in the vector.

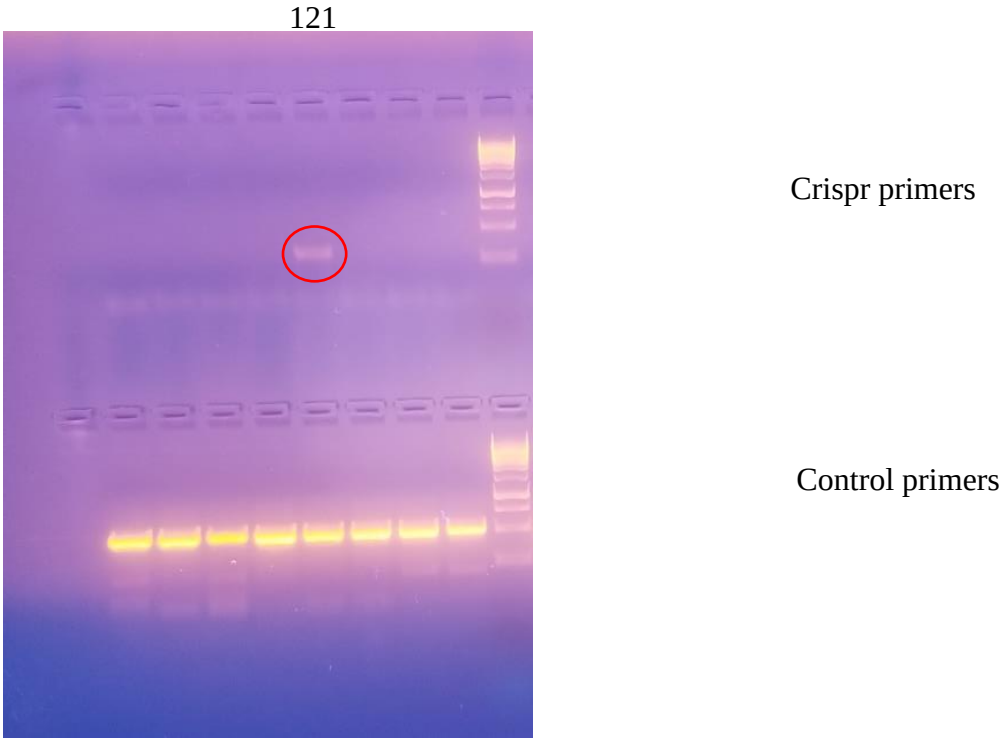

Figure 3.4: Genotyping of mCherry+ seeds in Arabidopsis thaliana

PCR was utilized to amplify DNA extracted from mCherry+ seeds. f-box1/f-box 4 double knockouts were transformed using a CRISPR construct targeted to F-box 3. Lines were genotyped utilizing primers flanking the F-box3. Resulting band at approximately 250 bp is indicative of F-Box 3 gene cut by CRIPR construct. CPK3 primers were used in tandem with CRISPR primers as a control.

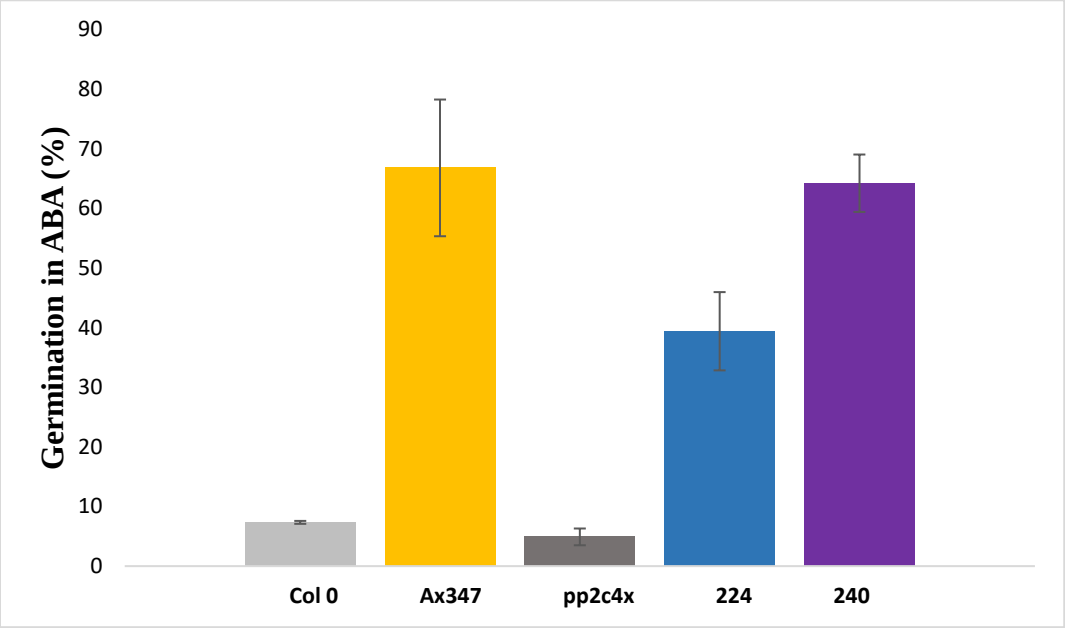

Figure 3.5: fbox 1,3,4 knock out lines were shown to demonstrate amiRNA line 347-like phenotype.

f-box 1,3,4 triple mutant lines were grown alongside Col 0, HsMYO, *pp2c* quadruple knockout, and the line identified in the amiRNA screen, Ax347 as controls. All lines were grown on ½ MS containing media, and ½ MS and 0.75 μM ABA containing plates. Quantification of germination was calculated after 8 days of exposure.

3.3 Discussion:

Artificial microRNA (amiRNA) lines are useful to circumvent redundancy and possible compensation by other closely related genes. This works by use of an amiRNA strand containing 21 nucleotides that will only target RNA with a corresponding sequence and no more than 5 mismatches, allowing for targeted knock-downs with fewer off-targets than previous methods (Schwab et al., 2006). This can be exploited by utilizing an amiRNA to target RNA strands from a group of genes that share sequence similarity. Previous lab members conducted a screen of a library of amiRNA transformed lines looking for those that would germinate well even in the presence of exogenous ABA (Hauser et al., 2019). During this screen, one of the lines showing much higher germination when compared to the wildtype was identified as line amiRNA-347 (AX347) (Figure 3.1). The higher germination rates when grown on ABA containing media was indicative of reduced sensitivity, as ABA promotes seed dormancy and inhibits germination (Finkelstein et al., 2002). Following sequencing of the amiRNA from line 347, it was shown to have targeted 5 of the F-Box genes, a family of over 700 genes.

As the amiRNA targeted 5 genes with unknown functions, determination of which genes were necessary and sufficient to recover the phenotype were required. A double mutant of *f-box 1/f*-box4 was generated as they were shown to be the most likely to interact with the ABA pathway in a meaningful manner based on preliminary experimentation. A germination assay was completed with the double mutant and appropriate controls, but the amiRNA phenotype was shown to be more robust than that observed in the double mutant. Therefore, in an effort to regain the previous phenotype a triple mutant was generated.

The triple mutant was created by transforming the *f-box1/f-box4* double mutant line with a CRISPR construct targeting *F-Box 3* with a vector obtained from Dr. Yunde Zhao. Identification of CRISPR+ lines was done through selection of mCherry+ seeds under a fluorescent microscope, and subsequent PCR-based genotyping of over 250 individual plants (Figure 3.2). Those that were shown to contain the truncated *f-box3* (Figure 3.4) were taken into the following generation. Seeds were reselected under the microscope, those that no longer fluoresced were selected for as they should no longer contain the CRISPR construct. Non-glowing seeds were selected and surface sterilized to be used for further genotyping. Genotyping will consist of re-confirming lines contain the cut *f-box3* gene; and positive lines will undergo a subsequent PCR to test for homozygosity by using primers that will amplify a region normally contained within the uncut gene. Another germination assay using seeds obtained from all 3 lines shown to have sustained the cut in T1 with appropriate controls is has been pursued in tandem. The assay allowed for quantification of germination on ABA containing media by all 3 lines identified and allow for comparison to the original amiRNA AX-347. As germination was shown to

Germination of at least one line taken into T2 appears to be homozygous based on phenotyping, and the phenotype observed in AX347 appears to have been recovered by that mutant line. F-box genes have been shown to contribute to a number of biological processes including stress responses, flowering, senescence, and even involvement in the ubiquitin-proteasome pathway (Stefanowicz et al., 2016). As it is already known that by creating mutant lines of these *F-Box* genes reduced ABA sensitivity can be observed, as they were discovered through a screen looking for ABA insensitive mutants. Therefore, when functional they must contribute to the ABA signaling pathway in a meaningful manner.

It has been hypothesized that these genes may target negative regulators of the pathway for degredation, leading to reduced sensitivity when nonfunctional, as observed. This hypothesis was based on their roles in other pathways, such as controlling relative amounts of upstream substrates, and their known interaction with the ubiquitin-proteasome pathway (Gonzalez et al., 2017; Hellmann & Estelle, 2002; Yan et al., 2013). However, before making any conclusions about their specific role in the pathway more experiments will be required, beginning with confirmation that a homozygous line has been isolated in T2.

3.4 Methods:

1. Germination Assays
2. Licor gas exchange experiments
3. Seed selection and growth conditions
4. DNA extraction and PCR-based genotyping

3.4.1 Germination Assays

Dr Paulo H. O. Ceciliato and Dr. Felix Hauser completed a screen of an ami-RNA library of seeds on ABA containing media. amiRNA-HsMYO which does not have a target gene in *Arabidopsis thaliana* was used as a control. Seeds were surface sterilized using either a 70% ethanol solution, or 50 mL bleach, 50 mL water and 50 µl Tween20 solution, followed by a minimum of 3 washes with water. Plants were grown on plates containing ½ MS (Murashige and Skoog Basal w/Gamborg Vitamins), 2.6 mM MES with potassium hydroxide (pH adjusted to 5.8) Phytoagar, and 0.5 µM ABA. After plating seeds were cold treated at 4℃ for 2-5 days before transfer to the growth room to be grown under 16 hours light: 8 hours dark light. Images were taken over the course of 7 days and quantification of germination was done utilizing the "Cell Counter" function within Image J software to analyze the images allowing for further analysis including calculation of percent germination.

3.4.2 Licor gas exchange experiments

Stomatal conductance (gs) was measured using single intact leaves from 5 to 6 week old healthy plants using a gas exchange analyzer (LI-6400 and LI-6800, LI-COR, Lincoln, NE, USA)

after allowing the plants to equilibrate for 1 hour. Experimentation was done under ambient CO_2 concentration of 400 ppm, 70-72% humidity, and light intensity of 150 μmol m^{-2} s^{-1} (10% blue light) at 21℃. Steady state stomatal conductance 10 minutes before the addition of ABA was recorded at respective concentrations (Hauser et al., 2019).

3.4.3 Seed selection and growth conditions

f-box1/f-box4 stable double mutant lines were transformed by Dr. Paulo H. O. Ceciliato using a Crispr construct targeting *F-box 3* utilizing a vector obtained from Dr. Yunde Zhao containing mCherry+. Seeds obtained from transformed plants were observed under the fluorescence microscope. Seeds that were transformed with the Crispr construct fluoresced red under the microscope when exposed to green light. Fluorescent seeds were selected for. Selected seeds were surface sterilized using sterilization solution (50 ml bleach, 50 ml water, 50 μl Tween20), and grown on ½ MS (Murashige and Skoog Basal w/Gamborg Vitamins) media containing plates.

3.4.4 DNA extraction and PCR-based genotyping

Approximately 250 mCherry+ seedlings were grown on ½ MS media, then transferred to soil and underwent PCR based genotyping. DNA was extracted from a single leaf from each plant and placed into respective 1.5 ml microcentrifuge tubes along with a metal bead, and then placed into liquid nitrogen. Samples were then secured in the ball mill for a 1 minute 30 seconds at 28 cycles per second. Ground samples were placed back into liquid nitrogen and DNA was extracted following the Shorty g-DNA extraction protocol. Following DNA extraction, all samples were amplified using PCR with primers flanking *F-Box 3*. Primers flanking *F-Box 3* were used to allow

for verification through gel electrophoresis on a 2% agarose gel, only cut genes would show a band upon visualization of the gel. A positive result yielded a band at approximately 450 bp. Extension time was reduced to 1 minute; an insufficient amount of time for Taq polymerase to complete construction of the complimentary strand in plants possessing an uncut gene. A negative result was indicative of an uncut gene and did not show a band under visualization. CPK3 primers were used in tandem with Crispr specific primers during PCR; and products were also present in gel electrophoresis as positive controls. Following confirmation of Crispr+ plants, seeds were collected. Seeds from the T2 generation will be reselected under the fluorescence microscope and genotyped again in the next generation.

Chapter 3 is co-authored with Dr. Paulo Ceciliato. The thesis author was the primary author of these chapters.

Works Cited

Ainsworth, E. A., & Rogers, A. (2007). The response of photosynthesis and stomatal conductance to rising [CO 2]: Mechanisms and environmental interactions. In *Plant, Cell and Environment* (Vol. 30, Issue 3, pp. 258–270). John Wiley & Sons, Ltd. https://doi.org/10.1111/j.1365-3040.2007.01641.x

Asseng, S., Ewert, F., Martre, P., Rötter, R. P., Lobell, D. B., Cammarano, D., Kimball, B. A., Ottman, M. J., Wall, G. W., White, J. W., Reynolds, M. P., Alderman, P. D., Prasad, P. V. V., Aggarwal, P. K., Anothai, J., Basso, B., Biernath, C., Challinor, A. J., de Sanctis, G., Doltra, J., Fereres, E., Garcia-Vila, M., Gayler, S., Hoogenboom, G., Hunt, L. A., Izaurralde, R. C., Jabloun, M., Jones, C. D., Kersebaum, K. C., Koehler, A-K., Müller, C., Naresh Kumar, S., Nendel, C., O'Leary, G., Olesen, J. E., Palosuo, T., Priesack, E., Eyshi Rezaei, E., Ruane, A. C., Semenov, M. A., Shcherbak, I., Stöckle, C., Stratonovitch, P., Streck, T., Supit, I., Tao, F., Thorburn, P. J., Waha, K., Wang, E., Wallach, D., Wolf, J., Zhao, Z., & Zhu, Y. (2015). Rising temperatures reduce global wheat production. *Nature Climate Change*, *5*(2), 143–147. https://doi.org/10.1038/nclimate2470

Bergmann, D. C. (2004). Integrating signals in stomatal development. In *Current Opinion in Plant Biology* (Vol. 7, Issue 1, pp. 26–32). Elsevier Ltd. https://doi.org/10.1016/j.pbi.2003.10.001

Brkljacic, J., Grotewold, E., Scholl, R., Mockler, T., Garvin, D. F., Vain, P., Brutnell, T., Sibout, R., Bevan, M., Budak, H., Caicedo, A. L., Gao, C., Gu, Y., Hazen, S. P., Holt, B. F., Hong, S. Y., Jordan, M., Manzaneda, A. J., Mitchell-Olds, T., Mochida, K., Mur, L. A. J., Park, C., Sedbrook, J., Watt, M., Zheng, S. J., & Vogel, J. P. (2011). Brachypodium as a model for the grasses: Today and the future. *Plant Physiology*, *157*(1), 3–13. https://doi.org/10.1104/pp.111.179531

Ceciliato, P. H. O., Zhang, J., Liu, Q., Shen, X., Hu, H., Liu, C., Schäffner, A. R., & Schroeder, J. I. (2019). Intact leaf gas exchange provides a robust method for measuring the kinetics of stomatal conductance responses to abscisic acid and other small molecules in Arabidopsis and grasses. *Plant Methods*, *15*(1), 38. https://doi.org/10.1186/s13007-019-0423-y

Chater, C. C. C., Caine, R. S., Fleming, A. J., & Gray, J. E. (2017). Origins and evolution of stomatal development. *Plant Physiology*, *174*(2), 624–638. https://doi.org/10.1104/pp.17.00183

Christmann, A., Hoffmann, T., Teplova, I., Grill, E., & Müller, A. (2005). Generation of active pools of abscisic acid revealed by in vivo imaging of water-stressed arabidopsis. *Plant Physiology*, *137*(1), 209–219. https://doi.org/10.1104/pp.104.053082

Christmann, A., Weiler, E. W., Steudle, E., & Grill, E. (2007). A hydraulic signal in root-to-shoot signalling of water shortage. *Plant Journal*, *52*(1), 167–174. https://doi.org/10.1111/j.1365-313X.2007.03234.x

Daszkowska-Golec, A., & Szarejko, I. (2013). Open or close the gate - Stomata action under the control of phytohormones in drought stress conditions. In *Frontiers in Plant Science* (Vol. 4, Issue MAY). Frontiers Research Foundation. https://doi.org/10.3389/fpls.2013.00138

Davies, W. J., & Zhang, J. (1991). Root Signals and the Regulation of Growth and Development of Plants in Drying Soil. *Annual Review of Plant Physiology and Plant Molecular Biology*, *42*(1), 55–76. https://doi.org/10.1146/annurev.pp.42.060191.000415

Deng, G., Zhou, L., Wang, Y., Zhang, G., & Chen, X. (2020). Hydrogen sulfide acts downstream of jasmonic acid to inhibit stomatal development in Arabidopsis. *Planta*, *251*(2), 42. https://doi.org/10.1007/s00425-019-03334-9

Dettinger, M., Udall, B., & Georgakakos, A. (2015). Western water and climate change. *Ecological Applications*, *25*(8), 2069–2093. https://doi.org/10.1890/15-0938.1

Doheny-Adams, T., Hunt, L., Franks, P. J., Beerling, D. J., & Gray, J. E. (2012). Genetic manipulation of stomatal density influences stomatal size, plant growth and tolerance to restricted water supply across a growth carbon dioxide gradient. *Philosophical Transactions of the Royal Society B: Biological Sciences*, *367*(1588), 547–555. https://doi.org/10.1098/rstb.2011.0272

Engineer, C. B., Ghassemian, M., Anderson, J. C., Peck, S. C., Hu, H., & Schroeder, J. I. (2014). Carbonic anhydrases, EPF2 and a novel protease mediate CO2 control of stomatal development. *Nature*, *513*(7517), 246–250. https://doi.org/10.1038/nature13452

Engineer, C. B., Hashimoto-Sugimoto, M., Negi, J., Israelsson-Nordström, M., Azoulay-Shemer, T., Rappel, W. J., Iba, K., & Schroeder, J. I. (2016). CO2 Sensing and CO2 Regulation of Stomatal Conductance: Advances and Open Questions. In *Trends in Plant Science* (Vol. 21, Issue 1, pp. 16–30). Elsevier Ltd. https://doi.org/10.1016/j.tplants.2015.08.014

Fahad, S., Bajwa, A. A., Nazir, U., Anjum, S. A., Farooq, A., Zohaib, A., Sadia, S., Nasim, W., Adkins, S., Saud, S., Ihsan, M. Z., Alharby, H., Wu, C., Wang, D., & Huang, J. (2017). Crop production under drought and heat stress: Plant responses and management options. In *Frontiers in Plant Science* (Vol. 8, p. 1147). Frontiers Media S.A. https://doi.org/10.3389/fpls.2017.01147

Finkelstein, R. R., Gampala, S. S. L., & Rock, C. D. (2002). Abscisic acid signaling in seeds and seedlings. *Plant Cell*, *14*(SUPPL.), S15–S45. https://doi.org/10.1105/tpc.010441

García-Marqués, F., Trevisan-Herraz, M., Martínez-Martínez, S., Camafeita, E., Jorge, I., Lopez, J. A., Méndez-Barbero, N., Méndez-Ferrer, S., del Pozo, M. A., Ibáñez, B., Andrés, V.,

Sánchez-Madrid, F., Redondo, J. M., Bonzon-Kulichenko, E., & Vázquez, J. (2016). A novel systems-biology algorithm for the analysis of coordinated protein responses using quantitative proteomics. *Molecular and Cellular Proteomics*, *15*(5), 1740–1760. https://doi.org/10.1074/mcp.M115.055905

Gonzalez, L. E., Keller, K., Chan, K. X., Gessel, M. M., & Thines, B. C. (2017). Transcriptome analysis uncovers Arabidopsis F-BOX STRESS INDUCED 1 as a regulator of jasmonic acid and abscisic acid stress gene expression. *BMC Genomics*, *18*(1). https://doi.org/10.1186/s12864-017-3864-6

Harrison, E. L., Arce Cubas, L., Gray, J. E., & Hepworth, C. (2020). The influence of stomatal morphology and distribution on photosynthetic gas exchange. In *Plant Journal* (Vol. 101, Issue 4, pp. 768–779). Blackwell Publishing Ltd. https://doi.org/10.1111/tpj.14560

Hashimoto, M., Negi, J., Young, J., Israelsson, M., Schroeder, J. I., & Iba, K. (2006). Arabidopsis HT1 kinase controls stomatal movements in response to CO2. *Nature Cell Biology*, *8*(4), 391–397. https://doi.org/10.1038/ncb1387

Hauser, F., Ceciliato, P., Lin, Y.-C., Guo, D., Gregerson, J. D., Abbasi, N., Youhanna, D., Park, J., Dubeaux, G., Shani, E., Poomchongkho, N., & Schroeder, J. I. (2019). A seed resource for screening functionally redundant genes and isolation of new mutants impaired in CO2 and ABA responses. *Journal of Experimental Botany*, *1*(22), 8–12. https://doi.org/10.1093/jxb

Hauser, F., Chen, W., Deinlein, U., Chang, K., Ossowski, S., Fitz, J., Hannon, G. J., & Schroeder, J. I. (2013). A genomic-scale artificial MicroRNA library as a tool to investigate the functionally redundant gene space in arabidopsis. *Plant Cell*, *25*(8), 2848–2863. https://doi.org/10.1105/tpc.113.112805

Hauser, F., Li, Z., Waadt, R., & Schroeder, J. I. (2017). SnapShot: Abscisic Acid Signaling. In *Cell* (Vol. 171, Issue 7, pp. 1708-1708.e0). Cell Press. https://doi.org/10.1016/j.cell.2017.11.045

Headquarters, N. (2014). *2014 NASA Strategic Plan*. www.nasa.gov

Hellmann, H., & Estelle, M. (2002). Plant development: Regulation by protein degradation. In *Science* (Vol. 297, Issue 5582, pp. 793–797). American Association for the Advancement of Science. https://doi.org/10.1126/science.1072831

Hetherington, A. M., & Woodward, F. I. (2003). The role of stomata in sensing and driving environmental change. In *Nature* (Vol. 424, Issue 6951, pp. 901–908). Nature Publishing Group. https://doi.org/10.1038/nature01843

Hiyama, A., Takemiya, A., Munemasa, S., Okuma, E., Sugiyama, N., Tada, Y., Murata, Y., & Shimazaki, K. I. (2017). Blue light and CO2 signals converge to regulate light-induced

stomatal opening. *Nature Communications*, *8*(1). https://doi.org/10.1038/s41467-017-01237-5

Hõrak, H., Sierla, M., Tõldsepp, K., Wang, C., Wang, Y. S., Nuhkat, M., Valk, E., Pechter, P., Merilo, E., Salojärvi, J., Overmyer, K., Loog, M., Brosché, M., Schroeder, J. I., Kangasjärvi, J., & Kollist, H. (2016). A dominant mutation in the ht1 kinase uncovers roles of MAP kinases and GHR1 in CO2-induced stomatal closure. *Plant Cell*, *28*(10), 2493–2509. https://doi.org/10.1105/tpc.16.00131

Hsu, P. K., Takahashi, Y., Munemasa, S., Merilo, E., Laanemets, K., Waadt, R., Pater, D., Kollist, H., & Schroeder, J. I. (2018). Abscisic acid-independent stomatal CO2 signal transduction pathway and convergence of CO2 and ABA signaling downstream of OST1 kinase. *Proceedings of the National Academy of Sciences of the United States of America*, *115*(42), E9971–E9980. https://doi.org/10.1073/pnas.1809204115

Hu, H., Boisson-Dernier, A., Israelsson-Nordström, M., Böhmer, M., Xue, S., Ries, A., Godoski, J., Kuhn, J. M., & Schroeder, J. I. (2010). Carbonic anhydrases are upstream regulators of CO2-controlled stomatal movements in guard cells. *Nature Cell Biology*, *12*(1), 87–93. https://doi.org/10.1038/ncb2009

Huo, N., Vogel, J. P., Lazo, G. R., You, F. M., Ma, Y., McMahon, S., Dvorak, J., Anderson, O. D., Luo, M. C., & Gu, Y. Q. (2009). Structural characterization of Brachypodium genome and its syntenic relationship with rice and wheat. *Plant Molecular Biology*, *70*(1–2), 47–61. https://doi.org/10.1007/s11103-009-9456-3

Jakobson, L., Vaahtera, L., Tõldsepp, K., Nuhkat, M., Wang, C., Wang, Y. S., Hõrak, H., Valk, E., Pechter, P., Sindarovska, Y., Tang, J., Xiao, C., Xu, Y., Gerst Talas, U., García-Sosa, A. T., Kangasjärvi, S., Maran, U., Remm, M., Roelfsema, M. R. G., Hu, H., Kangasjärvi, J., Loog, M., Schroeder, J. I., Kollist, H., & Brosché, M. (2016). Natural Variation in Arabidopsis Cvi-0 Accession Reveals an Important Role of MPK12 in Guard Cell CO2Signaling. *PLoS Biology*, *14*(12), 2000322. https://doi.org/10.1371/journal.pbio.2000322

Kanemoto, K., Yamashita, Y., Ozawa, T., Imanishi, N., Nguyen, N. T., Suwa, R., Mohapatra, P. K., Kanai, S., Moghaieb, R. E., Ito, J., El-Shemy, H., & Fujita, K. (2009). Photosynthetic acclimation to elevated CO2 is dependent on N partitioning and transpiration in soybean. *Plant Science*, *177*(5), 398–403. https://doi.org/10.1016/j.plantsci.2009.06.017

Kang, J., Hwang, J. U., Lee, M., Kim, Y. Y., Assmann, S. M., Martinoia, E., & Lee, Y. (2010). PDR-type ABC transporter mediates cellular uptake of the phytohormone abscisic acid. *Proceedings of the National Academy of Sciences of the United States of America*, *107*(5), 2355–2360. https://doi.org/10.1073/pnas.0909222107

Kaul, S., Koo, H. L., Jenkins, J., Rizzo, M., Rooney, T., Tallon, L. J., Feldblyum, T., Nierman, W., Benito, M. I., Lin, X., Town, C. D., Venter, J. C., Fraser, C. M., Tabata, S., Nakamura, Y., Kaneko, T., Sato, S., Asamizu, E., Kato, T., Kotani H., Sasamoto, S., Ecker, J. R., Theologis, A., Federspiel, N. A., Palm, C. J., Osborne, B. I., Shinn, P., Conway, A. B., Vysotskaia, V. S., Dewar, K., Conn, L., Lenz, C. A., Kim, C. J., Hansen, N. F., Liu, S. X., Buehler, E., Altafi, H., Sakano, H., Dunn, P., Lam, B., Pham, P. K., Chao, Q., Nguyen, M., Yu, G., Chen, H., Southwick, A., Lee, J., Miranda, M., Toriumi, M. J., Davis, R. W., Wambutt, R., Murphy, G., Düsterhöft, A., Stiekema, W., Pohl, Entian, K.-D., Terryn, N., Volckaert, G., Salanoubat, M., Choisne, N., Reiger, M., Ansorge, W., Unseld, M., Fartmann, B., Valle, G., Artiguenave, F., Weissenbach, J., Quetier, F. Wilson, R. K., de la Bastide, M., Sekhon, M., Huang, E., Spiegel, L., Gnoj, L., Pepin, K., Murray, J., Johnson, D., Habermann, K., Dedhia, N., Parnell, L., Preston, R., Hillier, L., Chen, E., Marra, M., Martienssen, R., McCombie, R., Mayer, K., White, O., Bevan, M., Lemcke, K., Creasy, T. H., Bielke, C., Haas, B., Maiti, Rama, Rudd, S., Peterson, J., Schoof, H., Frishman, D., Morgenstern, B., Zaccaria, P., Ermolaeva, M., Pertea, M., Quackenbush, J., Volfosky, N., Wu, D., Lowe, T. M., Salzberg, S. L., Mewes, H-W., Rounsley, S., Bush, D., Subramanaim, S., Levin, I., Norris, S., Schmidt, R., Acarkan, A., Bancroft, I, Quetier, F., Brennicke, A., Eisen, J. A., Bureau, T., Legault, B.-A., Le, Q.-H., Agrawal, N., Yu, Z., Martienssen, R., Copenhaver, G. P., Luo, S., Pikaard, C. S., Preuss, D., Paulsen, I. T., Sussman, M., Britt, A. B., Eisen, J. A., Selinger, D. A., Pandey, R., Mount, D. W., Chandler, V. L., Jorgensen, R. A., Pikaard, C., Jurgens, G., Meyerowitz, E. M., Ecker, J. R., Theologis, A., Dangl, J., Jones, J. D. G., Chen, M., Chory, J., & Somerville, C. (2000). Analysis of the genome sequence of the flowering plant Arabidopsis thaliana. *Nature*, *408*(6814), 796–815. https://doi.org/10.1038/35048692

Kollist, H., Nuhkat, M., & Roelfsema, M. R. G. (2014). Closing gaps: Linking elements that control stomatal movement. In *New Phytologist* (Vol. 203, Issue 1, pp. 44–62). Blackwell Publishing Ltd. https://doi.org/10.1111/nph.12832

Kuromori, T., Miyaji, T., Yabuuchi, H., Shimizu, H., Sugimoto, E., Kamiya, A., Moriyama, Y., & Shinozaki, K. (2010). ABC transporter AtABCG25 is involved in abscisic acid transport and responses. *Proceedings of the National Academy of Sciences of the United States of America*, *107*(5), 2361–2366. https://doi.org/10.1073/pnas.0912516107

Ma, Y., Szostkiewicz, I., Korte, A., Moes, D., Yang, Y., Christmann, A., & Grill, E. (2009). Regulators of PP2C phosphatase activity function as abscisic acid sensors. *Science*, *324*(5930), 1064–1068. https://doi.org/10.1126/science.1172408

Malcheska, F., Ahmad, A., Batool, S., Müller, H. M., Ludwig-Müller, J., Kreuzwieser, J., Randewig, D., Hänsch, R., Mendel, R. R., Hell, R., Wirtz, M., Geiger, D., Ache, P., Hedrich, R., Herschbach, C., & Rennenberg, H. (2017). Drought-enhanced xylem sap sulfate closes stomata by affecting ALMT12 and guard cell ABA synthesis. *Plant Physiology*, *174*(2), 798–814. https://doi.org/10.1104/pp.16.01784

Marriott, P. E., Sibout, R., Lapierre, C., Fangel, J. U., Willats, W. G. T., Hofte, H., Gómez, L. D., & McQueen-Mason, S. J. (2014). Range of cell-wall alterations enhance saccharification in Brachypodium distachyon mutants. *Proceedings of the National Academy of Sciences of the United States of America*, *111*(40), 14601–14606. https://doi.org/10.1073/pnas.1414020111

Mekonnen, M. M., & Hoekstra, A. Y. (2016). Sustainability: Four billion people facing severe water scarcity. *Science Advances*, *2*(2). https://doi.org/10.1126/sciadv.1500323

Negi, J., Matsuda, O., Nagasawa, T., Oba, Y., Takahashi, H., Kawai-Yamada, M., Uchimiya, H., Hashimoto, M., & Iba, K. (2008). CO2 regulator SLAC1 and its homologues are essential for anion homeostasis in plant cells. *Nature*, *452*(7186), 483–486. https://doi.org/10.1038/nature06720

Olsen, O., Wang, X., & von Wettstein, D. (1993). Sodium azide mutagenesis: Preferential generation of A·T → G·C transitions in the barley Ant18 gene. *Proceedings of the National Academy of Sciences of the United States of America*, *90*(17), 8043–8047. https://doi.org/10.1073/pnas.90.17.8043

Park, S. Y., Fung, P., Nishimura, N., Jensen, D. R., Fujii, H., Zhao, Y., Lumba, S., Santiago, J., Rodrigues, A., Chow, T. F. F., Alfred, S. E., Bonetta, D., Finkelstein, R., Provart, N. J., Desveaux, D., Rodriguez, P. L., McCourt, P., Zhu, J. K., Schroeder, J. I., Volkman, B. F., & Cutler, S. R. (2009). Abscisic acid inhibits type 2C protein phosphatases via the PYR/PYL family of START proteins. *Science*, *324*(5930), 1068–1071. https://doi.org/10.1126/science.1173041

Peterson, K. M., Rychel, A. L., & Torii, K. U. (2010). Out of the mouths of plants: The molecular basis of the evolution and diversity of stomatal development. In *Plant Cell* (Vol. 22, Issue 2, pp. 296–306). American Society of Plant Biologists. https://doi.org/10.1105/tpc.109.072777

Qiao, P., Bourgault, R., Mohammadi, M., Matschi, S., Philippe, G., Smith, L. G., Gore, M. A., Molina, I., & Scanlon, M. J. (2020). Transcriptomic network analyses shed light on the regulation of cuticle development in maize leaves. *Proceedings of the National Academy of Sciences of the United States of America*, *117*(22), 12464–12471. https://doi.org/10.1073/pnas.2004945117

Raissig, M. T., Abrash, E., Bettadapur, A., Vogel, J. P., & Bergmann, D. C. (2016). Grasses use an alternatively wired bHLH transcription factor network to establish stomatal identity. *Proceedings of the National Academy of Sciences of the United States of America*, *113*(29), 8326–8331. https://doi.org/10.1073/pnas.1606728113

Raissig, M. T., Matos, J. L., Gil, M. X. A., Kornfeld, A., Bettadapur, A., Abrash, E., Allison, H. R., Badgley, G., Vogel, J. P., Berry, J. A., & Bergmann, D. C. (2017). Mobile MUTE

specifies subsidiary cells to build physiologically improved grass stomata. *Science*, *355*(6330), 1215–1218. https://doi.org/10.1126/science.aal3254

Raschke, K., & Fellows, M. P. (1971). Stomatal movement in Zea mays: Shuttle of potassium and chloride between guard cells and subsidiary cells. *Planta*, *101*(4), 296–316. https://doi.org/10.1007/BF00398116

Rock, C. D., & Zeevaart, J. A. D. (1991). The aba mutant of Arabidopsis thaliana is impaired in epoxy-carotenoid biosynthesis. *Proceedings of the National Academy of Sciences of the United States of America*, *88*(17), 7496–7499. https://doi.org/10.1073/pnas.88.17.7496

Rowe, M. H., & Bergmann, D. C. (2010). Complex signals for simple cells: the expanding ranks of signals and receptors guiding stomatal development. In *Current Opinion in Plant Biology* (Vol. 13, Issue 5, pp. 548–555). Elsevier Current Trends. https://doi.org/10.1016/j.pbi.2010.06.002

Schneeberger, K., Ossowski, S., Lanz, C., Juul, T., Petersen, A. H., Nielsen, K. L., Jørgensen, J. E., Weigel, D., & Andersen, S. U. (2009). SHOREmap: Simultaneous mapping and mutation identification by deep sequencing. In *Nature Methods* (Vol. 6, Issue 8, pp. 550–551). Nature Publishing Group. https://doi.org/10.1038/nmeth0809-550

Scholthof, K. B. G., Irigoyen, S., Catalan, P., & Mandadi, K. K. (2018). Brachypodium: A monocot grass model genus for plant biology. In *Plant Cell* (Vol. 30, Issue 8, pp. 1673–1694). American Society of Plant Biologists. https://doi.org/10.1105/tpc.18.00083

Schroeder, J. I., & Hagiwara, S. (1989). Cytosolic calcium regulates ion channels in the plasma membrane of Vicia faba guard cells. *Nature*, *338*(6214), 427–430. https://doi.org/10.1038/338427a0

Schwab, R., Ossowski, S., Riester, M., Warthmann, N., & Weigel, D. (2006). Highly specific gene silencing by artificial microRNAs in Arabidopsis. *Plant Cell*, *18*(5), 1121–1133. https://doi.org/10.1105/tpc.105.039834

Seo, M., Hanada, A., Kuwahara, A., Endo, A., Okamoto, M., Yamauchi, Y., North, H., Marion-Poll, A., Sun, T. P., Koshiba, T., Kamiya, Y., Yamaguchi, S., & Nambara, E. (2006). Regulation of hormone metabolism in Arabidopsis seeds: Phytochrome regulation of abscisic acid metabolism and abscisic acid regulation of gibberellin metabolism. *Plant Journal*, *48*(3), 354–366. https://doi.org/10.1111/j.1365-313X.2006.02881.x

Seo, M., Nambara, E., Choi, G., & Yamaguchi, S. (2009). Interaction of light and hormone signals in germinating seeds. In *Plant Molecular Biology* (Vol. 69, Issue 4, pp. 463–472). Plant Mol Biol. https://doi.org/10.1007/s11103-008-9429-y

Sharp, R. E. (2002). Interaction with ethylene: Changing views on the role of abscisic acid in root and shoot growth responses to water stress. *Plant, Cell and Environment*, *25*(2), 211–222. https://doi.org/10.1046/j.1365-3040.2002.00798.x

Sherrard, M. E., & Maherali, H. (2006). THE ADAPTIVE SIGNIFICANCE OF DROUGHT ESCAPE IN AVENA BARBATA, AN ANNUAL GRASS. *Evolution*, *60*(12), 2478–2489. https://doi.org/10.1111/j.0014-3820.2006.tb01883.x

Stefanowicz, K., Lannoo, N., Zhao, Y., Eggermont, L., van Hove, J., al Atalah, B., & van Damme, E. J. M. (2016). Glycan-binding F-box protein from Arabidopsis thaliana protects plants from Pseudomonas syringae infection. *BMC Plant Biology*, *16*(1). https://doi.org/10.1186/s12870-016-0905-2

Steinwand, M., & Vogel, J. (2010). *Crossing Brachypodium*.

Stocker, T. F., Qin, D., Plattner, G.-K., Tignor, M. M. B., Allen, S. K., Boschung, J., Nauels, A., Xia, Y., Bex, V., & Midgley, P. M. (2013). *Climate Change 2013 The Physical Science Basis Summary for Policymakers Technical Summary Frequently Asked Questions Part of the Working Group I Contribution to the Fifth Assessment Report of the Intergovernmental Panel on Climate Change Edited by*.

Takahashi, Y., Zhang, J., Hsu, P. K., Ceciliato, P. H. O., Zhang, L., Dubeaux, G., Munemasa, S., Ge, C., Zhao, Y., Hauser, F., & Schroeder, J. I. (2020). MAP3Kinase-dependent SnRK2-kinase activation is required for abscisic acid signal transduction and rapid osmotic stress response. *Nature Communications*, *11*(1), 1–12. https://doi.org/10.1038/s41467-019-13875-y

Tõldsepp, K., Zhang, J., Takahashi, Y., Sindarovska, Y., Hõrak, H., Ceciliato, P. H. O., Koolmeister, K., Wang, Y.-S., Vaahtera, L., Jakobson, L., Yeh, C.-Y., Park, J., Brosche, M., Kollist, H., & Schroeder, J. I. (2018). Mitogen-activated protein kinases MPK4 and MPK12 are key components mediating CO2-induced stomatal movements. *The Plant Journal*, *96*(5), 1018–1035. https://doi.org/10.1111/tpj.14087

Vogel, J. P., Garvin, D. F., Mockler, T. C., Schmutz, J., Rokhsar, D., Bevan, M. W., Barry, K., Lucas, S., Harmon-Smith, M., Lail, K., Tice, H., Grimwood, J., McKenzie, N., Huo, N., Gu, Y. Q., Lazo, G. R., Anderson, O. D., You, F. M., Luo, M. C., Vogel, J. P., Dvorak, J., Wright, J., Febrer, M., Bevan, M. W., Idziak, D., Hasterok, R., Garvin, D. F., Lindquist, E., Wang, M., Fox, S. E., Priest, H. D., Filichkin, S. A., Givan, S. A., Bryant, D. W., Chang, J. C., Mockler, T. C., Wu, H., Wu, W., Hsia, A-P., Schnable, P. S., Kalyanaraman, A., Barbazuk, B., Michael, T. P., Hazen, S. P., Bragg, J. N., Laudencia-Chingcuaco, D., Vogel, J. P., Garvin, D. F., Weng, Y., Mckenzie, N., Bevan, M. W., Haberer, G., Spannagl, M., Mayer, K., Rattei, T., Mitros, T., Roksar, D., Lee, S-J, Rose, J. K. C., Mueller, L. A., York, T. L., Wicker, T., Buchmann, J. P., Tanskanen, J., Schulman, A. H., Gundlach, H., Wright, J., Bevan, M., Costa de Oliveira, A., Maia, L. C., Belknap, W., Gu, Y. Q., Jiang, N., Lai, J.,

Zhu, L., Ma, J., Sun, C., Pritham, E., Salse, J., Murat, F., Abrouk, M., Haberer, G., Spannagl, M., Mayer, K., Dvorak, J., Fahlgren, N., You, F. M., Luo, M-C., Dvorak, J., Fahlgren, N., Fox, S. E., Sullivan, C., M., Mockler, T. C., Carrington, J., C., Chapman, E. J., May, G. D., Zhai, J., Ganssmann, M., Guna Ranjan Gurazada, S., German, M., Meyers, B. C., Green, P. J., Bragg, J. N., Tyler, L., Wu, J., Gu, Y. G., Lazo, G. R., Laudencia-Chingcianco, D., Thomson, J., Hazen, S. P., Chen, S., Scheller, H. V., Harholt, J., Ulvskov, P., Fox, S. E., Silichkin, S. A., Kimbrell, J. A., Chang, J. H., Sullivan, C., M., Chapman, E. J., Carrington, J. C., Mockler, T. C., Bartley, L. E., Cao, P., Jung, K-H., Sharma, M. K., Vega-Sanchez, M., Ronald, P., Dardick, C. D., De Bolt, S., Verelst, W., Inze, D., Heese, M., Schnittger, A., Yang, X., Kalluri, U. C., Ouyang, S., Sun, Q., Liu, Z., Yilmaz, A., Grotewold, E., Sibout, R., Hematy, K., Mouille, G., Holte, H., Michael, T., Pelloux, J., O'Connor, D., Schnable, J., Walsh, S., Higgins, J., Bevan, M., Li, P., Brutnell, T., Unver, T., Budak, H., Belcram, H., Charles, M., Chalhoub, B., & Baxter, I. (2010). Genome sequencing and analysis of the model grass Brachypodium distachyon. *Nature*, *463*(7282), 763–768. https://doi.org/10.1038/nature08747

Vráblová, M., Vrábl, D., Hronková, M., Kubásek, J., & Šantrůček, J. (2017). Stomatal function, density and pattern, and CO2 assimilation in Arabidopsis thaliana tmm1 and sdd1-1 mutants. *Plant Biology*, *19*(5), 689–701. https://doi.org/10.1111/plb.12577

Wahid, A., Gelani, S., Ashraf, M., & Foolad, M. R. (2007). Heat tolerance in plants: An overview. In *Environmental and Experimental Botany* (Vol. 61, Issue 3, pp. 199–223). Elsevier. https://doi.org/10.1016/j.envexpbot.2007.05.011

Wang, C., Hu, H., Qin, X., Zeise, B., Xu, D., Rappel, W. J., Boron, W. F., & Schroeder, J. I. (2015). Reconstitution of CO2 regulation of SLAC1 anion channel and function of CO2-permeable PIP2;1 aquaporin as CARBONIC ANHYDRASE4 interactor. *Plant Cell*, *28*(2), 568–582. https://doi.org/10.1105/tpc.15.00637

Wang, Y., & Chen, Z. H. (2020). Does Molecular and Structural Evolution Shape the Speedy Grass Stomata? In *Frontiers in Plant Science* (Vol. 11). Frontiers Media S.A. https://doi.org/10.3389/fpls.2020.00333

Willmer, C., Fricker, M., Willmer, C., & Fricker, M. (1996). Stomatal responses to environmental factors. In *Stomata* (pp. 126–191). Springer Netherlands. https://doi.org/10.1007/978-94-011-0579-8_6

Woodward, A. W., & Bartel, B. (2018). Biology in bloom: A primer on the arabidopsis thaliana model system. *Genetics*, *208*(4), 1337–1349. https://doi.org/10.1534/genetics.118.300755

Woodward, F. I. (1987). Stomatal numbers are sensitive to increases in CO2 from pre-industrial levels. *Nature*, *327*(6123), 617–618. https://doi.org/10.1038/327617a0

Xu, Z., Jiang, Y., Jia, B., & Zhou, G. (2016). Elevated-CO2 response of stomata and its dependence on environmental factors. In *Frontiers in Plant Science* (Vol. 7, Issue MAY2016). Frontiers Media S.A. https://doi.org/10.3389/fpls.2016.00657

Xue, S., Hu, H., Ries, A., Merilo, E., Kollist, H., & Schroeder, J. I. (2011). Central functions of bicarbonate in S-type anion channel activation and OST1 protein kinase in CO2 signal transduction in guard cell. *EMBO Journal*, *30*(8), 1645–1658. https://doi.org/10.1038/emboj.2011.68

Yan, J., Li, H., Li, S., Yao, R., Deng, H., Xie, Q., & Xie, D. (2013). The Arabidopsis F-box protein CORONATINE INSENSITIVE1 is stabilized by SCFCOI1 and degraded via the 26S proteasome pathway. *Plant Cell*, *25*(2), 486–498. https://doi.org/10.1105/tpc.112.105486

Yang, Z., Liu, J., Tischer, S. v., Christmann, A., Windisch, W., Schnyder, H., & Grill, E. (2016). Leveraging abscisic acid receptors for efficient water use in Arabidopsis. *Proceedings of the National Academy of Sciences of the United States of America*, *113*(24), 6791–6796. https://doi.org/10.1073/pnas.1601954113

Yibing Wang, Geoffrey Holroyd, Alistair M Hetherinton, & Carl K-Y Ng. (2004). Seeing “cool” and ’hot’--infrared thermography as a tool for non-invasive, high-throughput screening of Arabidopsis guard cell signalling mutants. *Journal of Experimental Botany*, *1*(22), 8–12. https://doi.org/10.1093/jxb

Yu, Z., Zhang, D., Xu, Y., Jin, S., Zhang, L., Zhang, S., Yang, G., Huang, J., Yan, K., Wu, C., & Zheng, C. (2019). CEPR2 phosphorylates and accelerates the degradation of PYR/PYLs in Arabidopsis. *Journal of Experimental Botany*, *1*(22), 8–12. https://doi.org/10.1093/jxb

Zhang, J., Wang, N., Miao, Y., Hauser, F., McCammon, J. A., Rappel, W. J., & Schroeder, J. I. (2018). Identification of SLAC1 anion channel residues required for CO2/bicarbonate sensing and regulation of stomatal movements. *Proceedings of the National Academy of Sciences of the United States of America*, *115*(44), 11129–11137. https://doi.org/10.1073/pnas.1807624115

Zheng, Y., Li, F., Hao, L., Yu, J., Guo, L., Zhou, H., Ma, C., Zhang, X., & Xu, M. (2019). Elevated CO2 concentration induces photosynthetic down-regulation with changes in leaf structure, non-structural carbohydrates and nitrogen content of soybean. *BMC Plant Biology*, *19*(1), 255. https://doi.org/10.1186/s12870-019-1788-9